RESEARCH PAPER

EFFICACY OF SYNTHETIC SEDIMENT GRAPH DEVELOPED USING VARIOUS MODIFIED TIME-AREA METHODS

Azadeh Katebikord[1], Seyed H. Sadeghi[1*] and Vijay P. Singh[1, 2]

[1] Department of Watershed Management Engineering, Faculty of Natural Resources and Marine Sciences, Tarbiat Modares University, Noor, 46417-76489, Iran

[2] Department of Biological and Agricultural Engineering & Zachry Department of Civil & Environmental Engineering, Texas A&M University, College Station, TX 77843-2117, USA

***Corresponding author:** sadeghi@modares.ac.ir

Received: September 25th, 2021 / Accepted: April 24th, 2022 / Published: June 30th, 2022

https://DOI-10.24057/2071-9388-2021-109

ABSTRACT. Suspended sediment (SS) is an essential indicator for assessing watershed health. However, the temporal variation of SS, called sediment graph (SG) using readily available data, is not always considered, particularly in un-gauged watersheds, which are many in developing countries. Since field measurements of SS are time-consuming and costly, the synthetic SG seems to be a promising alternative. Therefore, it is essential to have reliable SS data for watershed management. This study aimed at simulating SGs through conceptual analysis of soil erosion and sediment yield at the watershed scale. To that end, soil erosion, sediment yield, and sediment routing were modeled using 38 storm events collected during 2011 and 2019 at the Galazchai Watershed in West Azerbaijan Province, Iran. Initially, the Time-Area Method (TAM) was applied, and then two strategies were considered to improve the TAM performance, including RUSLE and sediment delivery ratio (SDR) using gradient ratio and WaTEM/SEDEM methods. Comparing simulated SGs with recorded ones showed that the SDR-based method had the lowest relative error in time to peak and base time, but the peak value had the highest relative error. Results also showed that TAM developed using the spatially distributed travel time method had a better performance than the channel longitudinal profile method. Overall, TAM could not simulate the temporal variation of sediment and needs further research.

KEY WORDS: fluvial behavior, sediment modeling, soil erosion, temporal distribution, watershed modeling

CITATION: Katebikord A., Sadeghi S.H., Singh V.P. (2022). Efficacy of Synthetic Sediment Graph Developed using Various Modified Time-Area Methods. Geography, Environment, Sustainability, 2(15), p. 38-57
https://DOI-10.24057/2071-9388-2021-109

ACKNOWLEDGEMENTS: The corresponding author was partially supported by the Agrohydrology Research Group of Tarbiat Modares University (Grant No. IG-39713), Iran. The authors warmly credit Dr. Raoof Mostafazadeh, Dr. Pari Saeidi, and Dr. Mostafa Moradi Dashtpagerdi for providing the first data bank of rainfall storm occurrences.

Conflict of interests: The authors reported no potential conflict of interest.

INTRODUCTION

Soil erosion is a severe menace to soil and water resources. Soil erosion of watershed areas leads to suspended sediment (SS) and its transport by flow and sediment yield (Golosov et al. 2014; Sadeghi and Singh 2017). The spatio-temporal analysis of sediment yield is needed for watershed management, especially for soil and water conservation and watershed health assessment (Sadeghi et al. 2019; Hazbavi et al. 2020; Mirchooli et al. 2021). The amount of SS produced in a watershed depends on the distribution and duration of precipitation, sediment availability, flow velocity, geomorphology, land cover and human activities (Seeger et al. 2004; Messina and Biggs 2016; Rahaman and Solavagounder 2020; Sokolov et al. 2020; Waiyasusri and Wetchayont 2020; de Paula et al. 2021). Most watershed management studies provide general estimates of soil erosion using empirical or non-distributed models such as Universal Soil Loss Equation (USLE), Revised Universal Soil Loss Equation (RUSLE), and Water Erosion Prediction Project (WEPP) (Wischmeier and Smith 1978; Sadeghi and Mizuyama 2007; Srivastava et al. 2020; Zheng et al. 2020).

The pattern of SS variation during hydrological events, especially flood events, has already been considered (e.g., Rovira and Batalla 2006; Sadeghi et al. 2008b; Zheng et al. 2013; Sadeghi and Zakeri 2015; Sadeghi and Singh 2017; Rymszewicz et al. 2018; Zhan et al. 2019; Qiao et al. 2020). Since the SS load accounts for a significant portion of the total sediment load at the storm scale, the sediment load estimation from individual storms is of particular importance (Xie et al. 2017). Accordingly, the temporal distribution of the SS load as sediment graph (SG) at a storm-scale was considered (Sadeghi and Singh 2005; De Girolamo et al. 2015), based on sufficient sampling during each event (Rovira and Batalla 2006; Choubin et al. 2018; Ruben et al. 2020).

Different methods have been developed to estimate sediment yield at different temporal and spatial scales and provide synthetic SGs (Singh et al. 2008; Bhunya et al. 2010; Banasik and Hejduk 2014; Trinh et al. 2018). In estimating the temporal variation of SS for a storm, the Instantaneous Unit Hydrograph (IUH) has been used to produce Instantaneous Unit Sediment Graph (IUSG) and then provide SG (Banasik

and Mitchell 2008; Sadeghi et al. 2008; Bhunya et al. 2010; Banasik and Hejduk 2014). Other methods, such as regression analysis (Sadeghi and Saeidi 2010), power model (Bhunya et al. 2010), two-parameter gamma distribution function (Singh et al. 2013), and SCS-CN method with IUSG (Gupta et al. 2019), have also been used for deriving the synthetic SG. The SG has been simulated using hydrograph (Saeedi et al. 2016). Using 25 measured SGs from 2011 to 2015 in the Galazchai Watershed, Iran, Saeedi et al. (2016) simulated SG based on hydrograph with the allometric concept and fitted bivariate regression equations. Their results showed that the temporal components were more accurate than other components.

The spatial distribution of contributory areas in runoff generation was done using the time-area method (TAM) by Clark (1945). This method was then applied by Kothyari et al. (1994, 1996) to fluvial studies at the watershed scale. Noting the uncertainties of TAM in the estimation of SG (Kothyari et al. 1994, 1996; Du et al. 2009; Raisi et al. 2010; Sadeghi et al. 2015), Kothyari et al. 1994) divided the Karso watershed, India, into several segments based on TAM and used USLE to calculate erosion in each section, and then calculated the sediment transported to the watershed outlet with the sediment delivery ratio (SDR) derived from the slope ratio of the two consequent sections. Kothyari et al. (1997) also estimated instantaneous sediment variation for individual storms in 12 small watersheds in India by employing the kinematic wave method and sediment-based mapping, Kothyari et al. (2002), Sadeghi and Tofighi (2003), Raisi et al. (2010), Khaledi Darvishan et al. (2010) reported that the TAM was less than accurate. Her and Heatwole (2016) simulated sediment yield for three storm events in the Owl Run Watershed in the US using the HYSTAR model based on two time-area sediment routing methods and sediment transport capacity. Li et al. (2017) successfully examined monthly changes in sediment discharge and its amount in a watershed located in the karst areas of China. Mahoney et al. (2018) investigated the temporal and spatial variations of sediment production in the Upper South Elkhorn Watershed in Kentucky, USA. They found that the sediment production in different parts of the watershed was in proportion to the extent of their connection during the year. Gupta et al. (2019) modeled the SG for small watersheds using soil moisture under four different conditions in six watersheds, and the estimated values were compared with observed values and the Bhunya et al. (2010) Sediment Graph Model (BSGM). Ruben et al. (2020) used Acoustic Sediment Estimation Toolbox (ASET) to calculate SS transport in the Paraná River in Argentina to obtain temporal and spatial variations of SSC. Bajirao et al. (2021) validated the ANN and ANFIS Artificial Intelligence models to simulate the daily SSC of the Koyna River in India and showed that data preprocessing with wavelet significantly improved the model prediction. Yadav et al. (2021) used GA-MOO-ANN, ANN, MLR, and SRC models to estimate the suspended sediment at 11 gauging stations of the Mahanadi River, India from 1990 to 2010, and showed that the GA-MOO-ANN model was better than other models.

Despite the importance of temporal variation of SS load, SGs are not available in many watersheds. Therefore, a simple method based on readily available SG at the watershed scale is needed. To that end, TAM, due to its simplicity and easy availability of data, is desirable. However, it requires improvement, so TAM was derived from different approaches at the watershed scale. Hence, this study calculated isochrones using spatially distributed travel time and channel longitudinal profile methods using two methods, viz. Hadley et al. (1985) and WaTEM/SEDEM method to calculate the SDR for the increased accuracy of the TAM method in estimating the synthetic SG.

MATERIALS AND METHODS

Study area

The study was conducted in the Galazchai Watershed due to reliable information and input data (i.e., Sadeghi et al. 2015; Moradi Dashtpagerdi et al. 2019). The Galazchai Watershed (ca. 103 km^2, 37° 01' and 37° 09' N, and 44° 56' and 45° 35' E) is located in West Azerbaijan Province, Iran, as one of the sub-watersheds of the diminishing Urmia Lake. The general view of the study watershed is shown in Fig. 1. The mainstream is 19.3 km long. The mean slope is 32%, and the elevation varies from 1492 to 3273 m above mean sea level. The watershed is in a semiarid climate with a mean annual temperature of 11.8°C and mean annual precipitation (1981–2010) of 482 mm. The mean annual discharge of the Galazchai River is 1.64 m^3 s^{-1}, and the mean annual water yield is 51.72 million m^3, and the highest observed mean annual discharge was recorded at 7.24 m^3 s^{-1} (Sadeghi et al. 2015). Rangeland is the dominant vegetation of the area (≈ 87%). In many flat areas, land use is agriculture and orchard (≈ 11%). Most of the agricultural lands are distributed in the vicinity of the main outlet and upstream of the watershed (Sadeghi et al. 2015).

Methodology

Data Collection

In this study, TAM was used to prepare a synthetic SG. For this purpose, flow and SS data were also recorded for 38 storm events during 2011 and 2019. The storms from 2011 to 2018 were obtained from previous researches (i.e., Mostafazadeh et al. 2015; Saeedi et al. 2016; Moradi Dashtpagerdi et al. 2019), and the last 4 storms for year 2019 were recorded during the present study. All samplings were made from the onset of the rising flow at the main outlet to the time of flow recession. So that, the suspended sediment sampling was performed at one-hour intervals in each storm event. The water level was simultaneously recorded to estimate flow discharge using the associated stage-discharge relationship. Water samples for the determination of SS concentration were collected through the depth integration method with the help of 2 l-capacity polyethylene flasks. SS concentrations were then determined in g l^{-1} through settling, decantation, and drying processes in the oven at 105°C for 24 h (Putjaroon and Pongboon 1987; Walling et al. 2001; Sadeghi and Saeidi 2010).

Development of Isochrones

The watershed was subdivided into isochrone segments by spatially distributed travel time (Welle and Woodward 1986) and channel longitudinal profile methods as in Eq. (1):

$$T_c = \frac{Kc}{I^{0.4}}\left(\frac{nL}{\sqrt{S}}\right)^{0.6} \quad (1)$$

where T_c is the surface flow travel time (min), *Kc* is the unit conversion factor and equals 6.943, I is the rainfall intensity (mm h^{-1}) with a 2-year return period and 24-hour rainfall duration, *n* is the roughness coefficient (Usul and Yilmaz 2002), *L* is the flow length (m), and *S* is the surface slope (m m^{-1}). The digital elevation model was used to calculate the slope and flow direction (FldrGrid) (Sadeghi et al. 2015).

The concentration time was calculated in the channel longitudinal profile method by the Kirpich formula (Sadeghi et al. 2015) as in Eq. (2).

$$T_c = 0.6628 L^{0.77} S^{-0.385} \quad (2)$$

where *Tc* is the concentration time (h), *L* is the stream length (km), and S is the typical slope (m m^{-1}). The principal tributary profiles and contour lines were plotted on the topographic map at a spacing equal to the desired period of 0.5 h to create isochrones on the watershed map. TAH was calculated by computing areas between isochrones drawn by joining the points of intersections with the same time interval. The pattern of isochrone areas with a digital elevation model (DEM) as the background is shown in Fig. 1. DEM with 30 m resolution was downloaded from the Terra satellite ASTER sensor from the USGS. This DEM was used due to its availability for the study area whose precision and validity have been proved and also recommended by Moradi Dashtpagerdi et al. (2019) for the same study watershed.

Soil Erosion Estimation

The RUSLE model was used to compute soil erosion in each isochrone segment, as stated in the general form of Eq. (3) (Renard et al. 1991).

$$E = RKLSCP \quad (3)$$

in which *E* is estimated soil loss (ton ha^{-1}) for each storm, *R* is rainfall erosivity factor (Mj mm ha^{-1} h^{-1}), *K* is soil erodibility factor (ton ha h ha^{-1} Mj^{-1} mm^{-1}), *LS* is slope length and steepness factor, *C* is cover management factor, and *P* is conservation practice factor.

Since no details except the total amount precipitation has been recorded in the weather station nested in the watershed, the calibrated Roose method (Roose 1977) for the region (Sadeghi and Tavangar 2015; Sadeghi et al. 2017) was used to calculate rainfall erosivity (R in Mj mm ha^{-1} h^{-1}) using the amount of rainfall (P in mm) as shown in Eq. (4).

$$R_R = 0.5 + 0.05P \quad (4)$$

In the same vein, no soil study has been conducted for the region to be used for the current research. Meanwhile, the global soil maps do not have an appropriate resolution for the small study watershed. Therefore, a high-resolution soil sampling was made through which 88 soil samples were collected from different parts of the watershed whose details were employed to develop the *K* factor map. After performing relevant experiments to calculate soil texture and organic matter, the value was calculated using soil erodibility nomograph (Foster et al. 1981), and the values were generalized to the watershed surface using the kriging method (Arnaldo et al. 2018). The *L* factor was obtained using Eq. (5) as proposed by Desmet and Govers (1996). The results were then multiplied into S to ultimately obtain the *LS* factor for the Galazchai Watershed.

$$L = \frac{\left(A_{ij-in} + D^2\right)^{m+1} - A_{ij-in}^{m+1}}{D^{m+2} \times x_{ij}^{m} \times 22.13^{m}} \quad (5)$$

where is the contributing area (m^2), *D* is the dimension of each cell (m), and x_{ij}=*sin* a_{ij}+*cos* a_{ij} x a_{ij} is also the flow direction in each cell *ij*. To prepare input maps to SAGA GIS software, the catchment area tool, particular area raster map, and slope map were used (Khorsand et al. 2017). The slope map was obtained using the 9-parameter 2nd order polynomial method (Zevenbergen and Thorne 1987) in SAGA software with radian unit. Also, a multiple flow direction method was used to map A_{ij} due to its ability to simulate convex and concave flows (Desmet and Govers 1996). As shown in Eq. 6, the cover management factor (C) on storm basis was calculated using the Normalized Difference Vegetation Index (NDVI) (Durigon et al. 2014). In this study, the Landsat 8 Operational Land Imager (OLI) and the ETM+ sensor from the USGS site were used to obtain NDVI. Therefore, Landsat OLI was georeferenced and necessary corrections including radiometric and FLAASH atmospheric were consequently conducted. The panchromatic images were also used to increase the

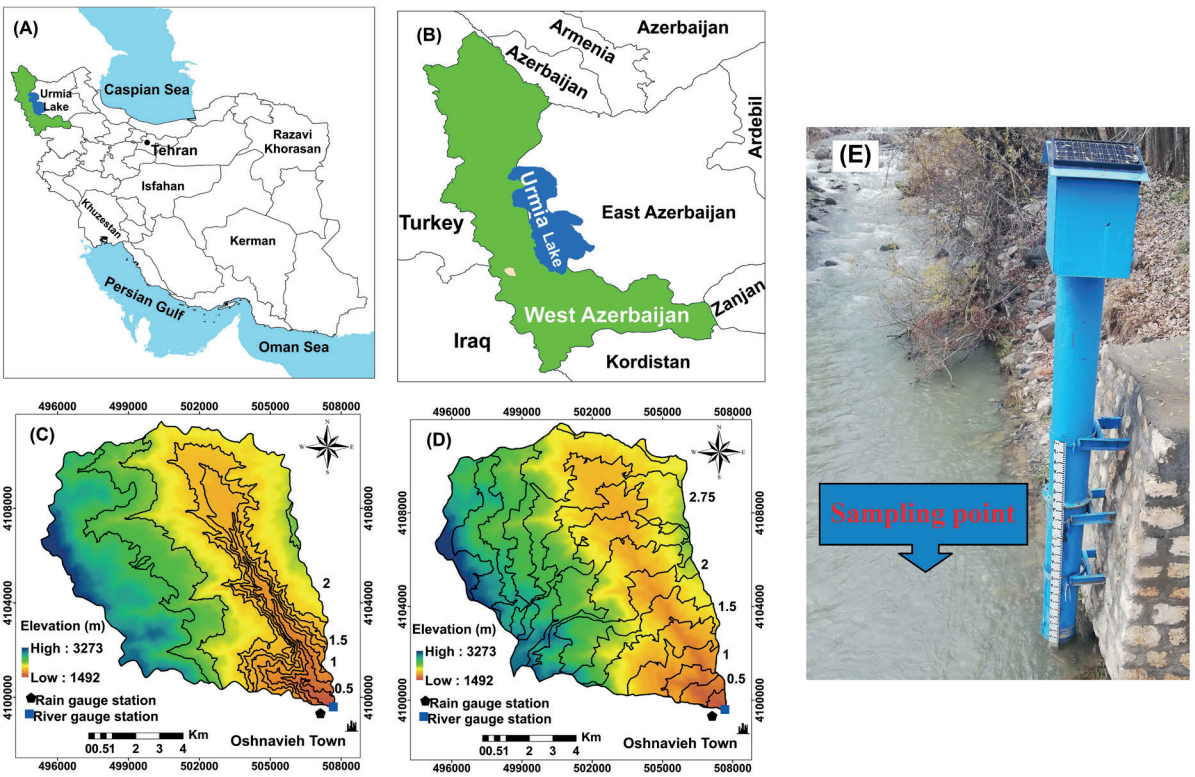

Fig. 1. A general view (A&B), the distribution pattern of the isochrone areas using the channel longitudinal profile (C), and spatially distributed travel time (D) methods with digital elevation model (DEM) as background with 30 m resolution (USGS), and a photo from the river gauge station (E) of the Galazchai Watershed, West Azerbaijan, Iran

resolution of images to 15 m (Hadjimitsis et al. 2010; Zhang et al. 2017). Ultimately, the red and near-infrared bands were used to prepare the NDVI. Since the time scale of a storm has been considered for the study, it was tried to use a satellite image for each storm to calculate the C factor. Nevertheless, due to the proximity of the occurrence date of the storms, the maximum number of six C factors was finally obtained. For example, for storms 35 and 36, a C factor was obtained, and for storms 37 and 38, another C factor was obtained.

$$C = 1 - NDVI / 2 \quad (6)$$

If no conservation practice is done, the P factor was deemed one (Wischmeier and Smith 1978). The land-use effect was also considered to further adjust the P factor to avoid overestimation of the amount of soil erosion (Panagos et al. 2015). Thus, for forest and rangeland, the value of P was one. In agriculture at different slopes, P values were considered 0.1 to 0.33. The maps used to estimate soil erosion using the RUSLE model are shown in Fig. 2. Rainfall erosivity for different storms is summarized in Table 2.

Sediment Routing

Sediment routing between two adjacent isochrone segments was obtained using the SDR concept developed, based on the slope ratio of the giving segment to the receivisng segment (Hadley et al. 1985). If the slope of the upstream isochrone was higher than the downstream, all the erosion that occurred would be transferred to the next segment as sediment, otherwise, SDR was equal to upstream segment slope per downstream segment slope. The temporal variations of sediment yield concerning the time of participation of the isochrone segments to the total sediment were also calculated.

The RUSLE-based WaTEM/SEDEM (i.e., Water and Tillage Erosion Model/Sediment Delivery Model) with similar inputs was also used to estimate SDR (Verstraeten et al. 2002). Sediment transport capacity (STc) was obtained from Eq. (7):

$$STc = ktc \times Eprg = ktc \times R \times K \times \left(LS - 4.12 \times Sg^{0.8} \right) \quad (7)$$

where *ktc* is the transport capacity coefficient, Eprg is the potential gully erosion, *R, K,* and *LS* are the RUSLE

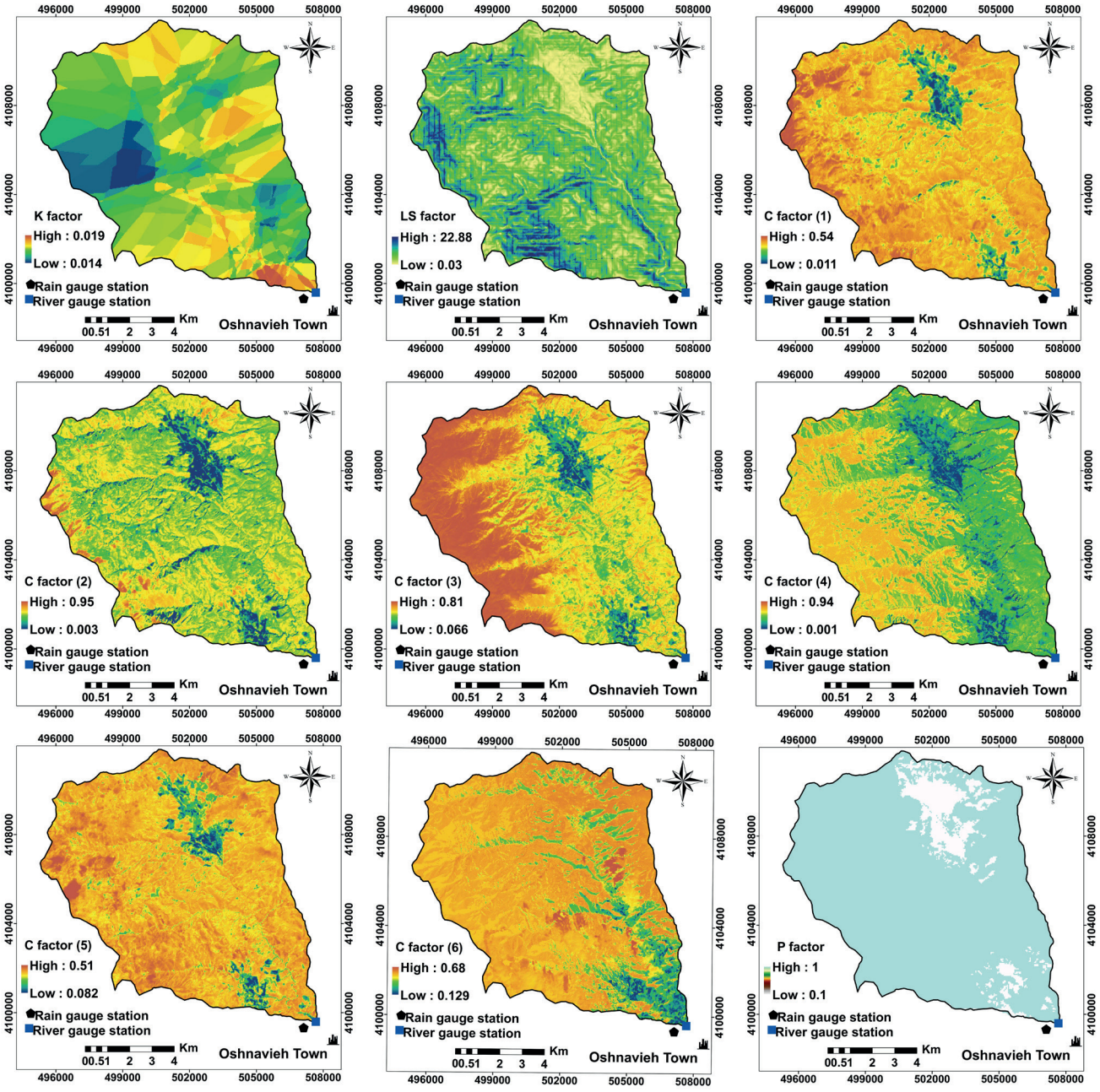

Fig. 2. Map of topography factor (LS), soil erodibility factor (K), Conservation practice factor (P), and cover management factor at different times (C) for the Galazchai Watershed, West Azerbaijan Province, Iran

factors, and *Sg* is the ground slope. The *ktc* is the main coefficient for calibrating the WaTEM/SEDEM model. In many documents (e.g., Quijano et al. 2016; Borrelli et al. 2018), changing this coefficient has been used to calibrate the model. The values of *ktc* should be calibrated for the use of the model. The sediment delivery ratio was calculated using the relationship presented in the WaTEM-SEDEM in GIS. It was determined that *ktc* values less than 0.5 should be checked. Because, when *ktc*>0.5, SDR was much higher than the unacceptable value of one. Therefore, *ktc* values less than 0.5 were examined with intervals of 0.01. The performance of the model was then determined using the median confidence level (*ME*) index (Borrelli et al., 2018). Therefore, by comparing the *ME* value, *ktc*=0.2 was finally considered for the subsequent calculations. After calculating *STc* (i.e., The transport capacity is the maximum sediment mass that can be transported by the overland flow), SDR was obtained using Eq. (8).

$$SDR = STc / SoilErosian \quad (8)$$

Sediment Graph Simulation

After calculating soil erosion in each isochrone and each storm, its temporal distribution was calculated using the lag time of each segment to the outlet and its cumulative contribution to sediment yield. The critical components of synthetic SGs, including base time, time to peak, and SSC peak, were compared with those of the observed SGs. Finally, the total sediment of each storm was

$$V_S = SDR_1E_1 + SDR_1SDR_2E_2 + ... + SDR_1SDR_2...SDR_nE_n \quad (9)$$

obtained using Eq. (9) (Kothyari et al. 1996):

where V_S is total sediment yield (t), SDR_i is sediment delivery ratio for each segment, and E_i is soil erosion in each isochrone segment (t).

Calibration and Validation of Synthetic Sediment Graph

According to the limited number of the recorded storm events, some 70% of the events were used for the calibration stage. The rest 30%, was employed for the validation stage (Dawson et al. 2007; Mohammed et al. 2021). Therefore, 38 storms were divided into two parts, 25 and 13. It is necessary to explain that there were 36 recorded storms at first, so 25 storms for calibration and 11 for validation were considered. Then, two more storms were further collected during the research and added to the validation stage. Data recorded from 2011 to 2014 were used for the calibration, and data recorded last two years of 2018 to 2019 ended at the time of preparation of the current report, and extendable to the near future were used for the validation. The simulated SGs were compared with recorded ones in terms of peak and total sediment volume, base time, and time to peak using absolute (*AE*) and relative (*RE*) errors. The overall performance of the estimated SGs was also assessed using the normalized Nash–Sutcliffe efficiency (NNSE) and root mean squared error (RMSE). These criteria were calculated for both calibration and validation datasets (Dawson et al. 2007; Nossent and Bauwens 2012; Sadeghi and Saeidi 2010). Finally, the best model performance in estimating SG components was selected based on the lowest AE, RE, and RMSE and highest NNSE (Dawson et al. 2007; Sadeghi et al. 2008; Sadeghi and Saeidi 2010). The Normalized Nash-Sutcliffe efficiency (*NNSE*) was employed for a more straightforward interpretation and to show how different methods actually worked. In this regard, Nash-Sutcliffe efficiencies of 1, 0, and -∞ correspond to *NNSE* of 1, 0.5, and 0, respectively (Nossent and Bauwens 2012).

RESULTS

To determine the efficacy of the time-area model (TAM), mean soil erosion was calculated for each storm. The characteristics of the 38 storm events from October 2011 to March 2019, rainfall erosivity, and mean soil erosion of each storm are shown in Table 2. As seen, the lowest and highest erosion rates were 0.02 and 0.047 (ton ha^{-1}), respectively, for the storms dated October 29, 2011, and March 31, 2019.

Then, the channel longitudinal profile and spatially distributed travel time were used to divide the watershed into isochrone segments. Sediment routing was also done by the Hadley et al. (1985) method. Details of each isochrone segment are given in Table one to ten is in the appendix. Therefore, the table numbers in the appendix should be corrected and written from Appendix 1 to Appendix 10. The table numbers will also change in the text of the manuscript. Though it can be rearranged based on the journal system and format too. The tables citations were fixed in the context. The SDR equaling one indicated that all soil eroded in the higher slope segment was transferred to the lower slope segment (Hadley et al. 1985; Kothyari et al. 1996). SDR was also calculated using WaTEM/SEDEM. The SDR results of the two methods for each isochrone segment are shown in Appendix Table 2.

Table 1. NNSE and RMSE results for different methods in two stages of calibration and validation for the Galazchai Watershed, Iran

Methods	Stage	Time to peak (h)		Peak Value (ton)		Base Time (h)		Total sediment (ton)	
		NNSE	RMSE	NNSE	RMSE	NNSE	RMSE	NNSE	RMSE
Hadley/channel longitudinal profile	Calibration	0.31	5.81	0.07	3699.98	0.19	13.91	0.45	3037.54
Hadley/spatially distributed travel time		0.31	5.92	0.30	1506.11	0.21	12.83	0.45	3074.39
WaTEM-SEDEM/channel longitudinal profile		0.31	5.81	0.49	996.77	0.19	13.91	0.45	3080.14
WaTEM-SEDEM/spatially distributed travel time		0.31	5.92	0.48	1027.01	0.21	12.83	0.45	3069.70
Hadley/channel longitudinal profile	Validation	0.29	9.20	0.01	458.18	0.16	17.52	0.44	371.93
Hadley/spatially distributed travel time		0.27	9.60	0.19	109.69	0.18	16.40	0.45	362.35
WaTEM-SEDEM/channel longitudinal profile		0.29	9.20	0.09	161.63	0.16	17.52	0.31	488.08
WaTEM-SEDEM/spatially distributed travel time		0.27	9.60	0.51	51.24	0.18	16.40	0.33	470.17

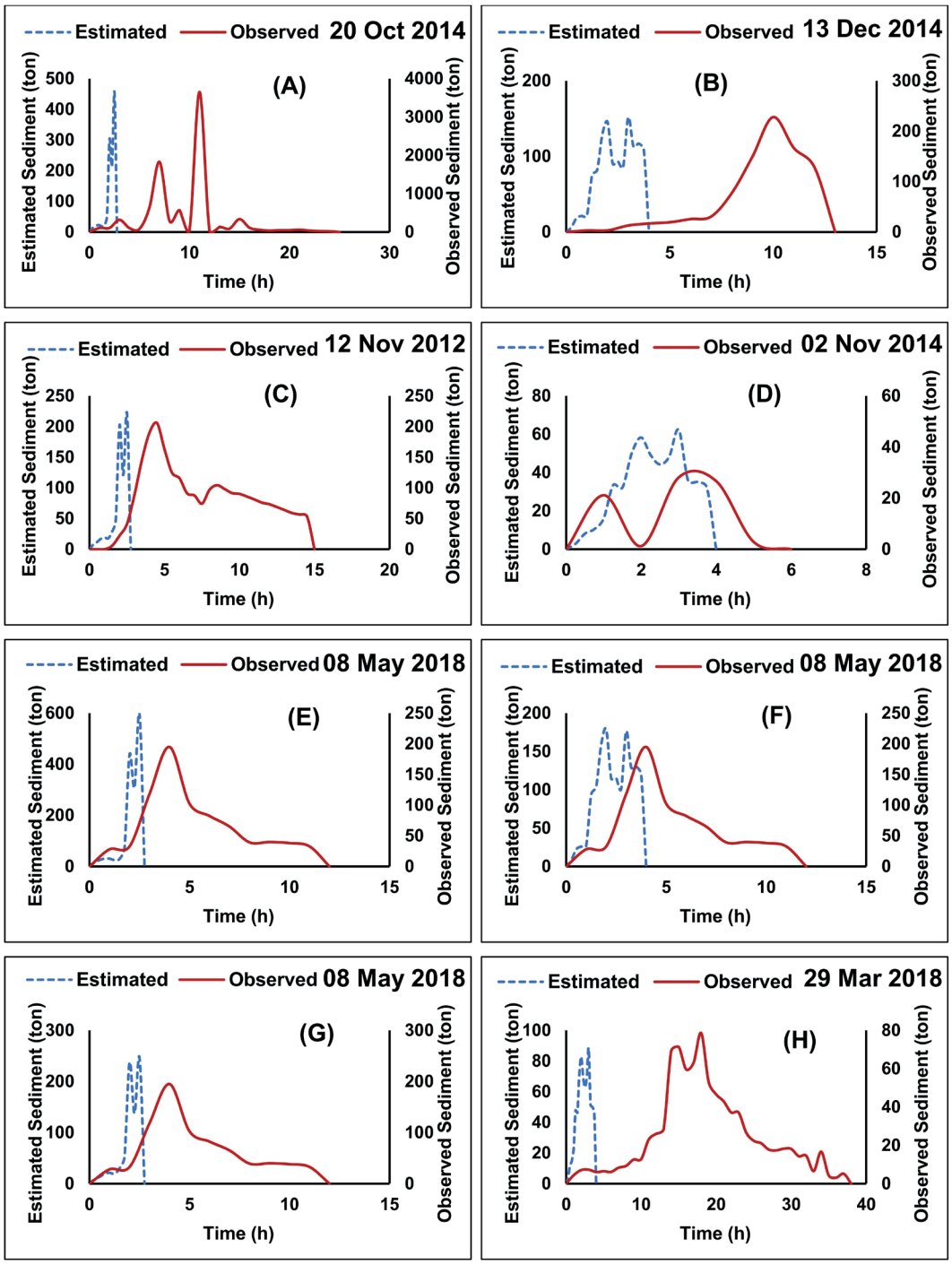

Fig. 3. Sample of synthetic sediment graphs obtained from different methods with the lowest RE in peak value estimation, (A)&(E): channel longitudinal profile and Hadley methods, (B)&(F): spatially distributed travel time and Hadley methods, (C)&(G): channel longitudinal profile and WaTEM/SEDEM, (D)&(H) methods: spatially distributed travel time and WaTEM/SEDEM methods

The results of TAMs derived from the channel longitudinal profile and spatially distributed travel time methods and corresponding sediment estimations are presented in Appendix Tables 3 to 10 for the calibration and validation data sets. Table 1 also shows the NNSE and RMSE results. Finally, sediment graphs were prepared. Fig. 2 shows some examples of synthetic sediment graphs obtained from different methods.

DISCUSSION

This study aimed to prepare synthetic sediment graphs in the Galazchai Watershed using readily available data, based on Kothyari et al. (1994 and 1997) and Kothyari et al. (2002). While they reported the accuracy of TAM in the simulation of SG in a small watershed in India, Sadeghi and Tofighi (2003) and Khaledi Darvishan et al. (2010) observed poor performance of the original TAM. To increase the accuracy in each stage of synthetic sediment graph preparation, the following modifications were made: (a) Soil erosion was calculated using RUSLE with each of its factors computed as accurately as possible. For example, six C factors were calculated for different storms. (b) For calculating the isochrone segments, two methods of longitudinal channel profile (Sadeghi et al. 2015) were used. (c) SDR was calculated using two Hadley et al. (1985) and WaTEM/SEDEM.

The minimum and maximum RE for the estimated peak values were 87.54 % and -161588.7 % for the channel longitudinal profile and Hadley et al. (1985) methods.

Likewise, the minimum and maximum *RE* for the estimated peak values were 33.58 % and -51521.1 % for the spatially distributed travel time and Hadley et al. (1985) methods. At the same time, the minimum and maximum *RE* for estimated peak values equaled -7.53 % and -8825 % for channel longitudinal profile and WaTEM/SEDEM. Ultimately, the least minimum and maximum *RE* for the estimated peak values belonged to the spatially distributed travel time method and WaTEM/SEDEM with respective values of 0.45 % and -3008.9 %. Similarly, the *RE* values ranged from 2.28 to -6273.7; 2.28 to -6273.7; -9.1 to -7026.1; 61.96 to 99.9, and -12.3 to 99.961 associated with channel longitudinal profile and Hadley et al. (1985) methods, spatially distributed travel time and Hadley et al. (1985) methods, channel longitudinal profile and WaTEM/SEDEM approach, and spatially distributed travel time method and WaTEM/SEDEM method, respectively. The negative *RE* values indicated an overestimation of the model. Despite the high error in estimating peak and total sediment, results showed that peak and base times were simulated with lower errors. In addition, the spatially distributed travel time method estimated the peak time and base time with lower error than did the channel longitudinal profile method.

The coefficient of variations varied from 0 to 139.1% for the simulated sediment graph obtained from different methods. Also, the standard deviations for the study criteria were from 0 to 2952.9. The lower coefficients of variation were related to time components, and the highest ones were related to peak value and total sediment. In general, the Hadley et al. (1985) estimates in both channel longitudinal profile and spatially distributed travel time methods in the calibration stage had the highest coefficient of variation and standard deviation. According to Table 11, none of the methods could reasonably estimate the various components of the sediment graph in all the mentioned methods. Results showed that the NNSE values were all less than 0.5, which indicated the low performance of different methods. The highest NSEE value, 0.49, was related to the peak value in the calibration stage, using the WaTEM-SEDEM/channel longitudinal profile method. Likewise, the lowest value of NSEE (i.e., 0.01) was related to the peak value obtained from the Hadley/channel longitudinal profile method in the validation stage. Similarly, the lowest value of RMSE, 5.81, was related to Hadley et al. (1985) and WaTEM-SEDEM/channel longitudinal profile, while the highest value of RMSE (i.e., 3699.98) was associated with the Hadley et al. (1985)/channel longitudinal profile method.

Results showed that in the calibration stage, channel longitudinal profile, WaTEM-SEDEM/channel longitudinal profile, spatially distributed travel time method, and Hadley et al. (1985)/channel longitudinal profile were more efficient for estimating time to peak, base time, peak value, and total sediment. In the validation stage, the estimation of time to peak by the channel longitudinal profile, the base time by the spatially distributed travel time method, the peak value by the WaTEM-SEDEM method/spatially distributed travel time, and the total sediment by Hadley/spatially distributed travel time was better performed.

Scrutinizing Table 2 showed that the WaTEM/SEDEM method reduced the SDR values by about 50% on average. In this method, SDR was calculated separately for each storm, and also factors than slope were considered. However, none of these methods had enabled TAM to simulate sediment graphs accurately. These results are consistent with the results of Sadeghi and Tofighi (2003) and Khaledi Darvishan et al. (2010) but are inconsistent with the results of Kothyari et al. (1994 and 1997) and Kothyari et al. (2002). Estimates of peak value and total sediment were, in most cases, more than observed values. High sediment estimation can be ascribed to the inaccuracy of the RUSLE method in estimating soil erosion in the study watershed because of rigorous topography and non-uniform distribution of rainfall (Khaledi Darvishan et al. 2010; Kothyari et al. 1997).

The time to peak and base time had lower coefficients of variation because these are mainly influenced by the physical characteristics of the watershed. The rest of the sediment graph components showed higher coefficients of variation due to precipitation conditions and other influential factors. These results are consistent with the findings reported by Mostafazadeh et al. (2015). The amount of relative error in estimating the peak values resulting from the WaTEM/SEDEM method had decreased by about 60% on average. The success of WaTEM/SEDEM results has been confirmed by Bezak et al. (2015) and Fang (2020). The ratio between sediment yield and soil erosion depends on many factors, for example, topography, climatic conditions, and geology (Bezak et al. 2015). Therefore, in this study, WaTEM/SEDEM was able to estimate with minor error than the Hadley et al. (1985) method. Besides, while employing WaTEM/SEDEM, SDR was calculated for each storm individually. As shown in Figure 2, although in these examples, different methods were able to estimate the peak value somewhat close to the observed value, they were not successful in simulating the overall sediment graphs shape. This disagreement was due to the effect of TAM structure on the overall shape of sediment graphs.

CONCLUSIONS

The present study synthesized SG using the modified TAM in the Galazchai Watershed, Iran. It can be concluded that, in general, TAM could not adequately simulate the temporal variation of sediment. Therefore, the methods of calculating SDR and isochrones were redefined, and the associated synthetic SGs were computed. The TAM performed better with the channel longitudinal profile method with the spatially distributed travel time method. It also had a better estimate of the time components than the sediment values. Overall, WaTEM/SEDEM performed better than the Hadley et al. (1985) method in SG components simulation.

REFERENCES

Adhami M., Sadeghi S.H.R., Duttmann R. and Sheikhmohammady M. (2019). Changes in watershed hydrological behavior due to land use comanagement scenarios. Journal of Hydrology, 577(July), 124001, DOI: 10.1016/j.jhydrol.2019.124001.

Arnaldo F., Avalos P., Gomes P.V., Leandro M., Silva N. and Oliveira M.S. De. (2018). Digital soil erodibility mapping by soilscape trending and kriging. Land Degradation & Development, 29(9), 3021–3028, DOI: 10.1002/ldr.3057.

Arnold J.G., Srinivasan R., Muttiah R.S. and Williams J.R. (1998). LARGE AREA HYDROLOGIC MODELING AND ASSESSMENT PART I : MODEL DEVELOPMENT. JAWRA Journal of the American Water Resources Association, 34(1), 73–89.

Bajirao T.S., Kumar P., Kumar M. and Elbeltagi A. (2021). Superiority of Hybrid Soft Computing Models in Daily Suspended Sediment Estimation in Highly Dynamic Rivers. Sustainability, 13(2), 542.

Banasik K. and Hejduk A. (2014). Ratio of basin lag times for runoff and sediment yield processes recorded in various environments. IAHS-AISH Proceedings and Reports, 367(December 2014), 163–169, DOI: 10.5194/piahs-367-163-2015.

Banasik K. and Mitchell J.K. (2008). Conceptual model of sedimentgraph from fl ood events in a small agricultural watershed. Annals of Warsaw University of Life Sciences-SGGW. Land Reclamation, 57(39), 49–57.

Bezak N., Rusjan S., Petan S., Sodnik J. and Mikoš M. (2015). Estimation of soil loss by the WATEM/SEDEM model using an automatic parameter estimation procedure. Environmental Earth Sciences, 74(6), 5245–5261, DOI: 10.1007/s12665-015-4534-0.

Bhunya p. k., Jain S.K., Singh P.K. and Mishra S.K. (2010). A simple conceptual model of sediment yield. Water Resources Management, 24(8), 1697–1716, DOI: 10.1007/s11269-009-9520-4.

Borrelli P., Oost K. Van, Meusburger K., Alewell C., Lugato E. and Panagos P. (2018). A step towards a holistic assessment of soil degradation in Europe : Coupling on-site erosion with sediment transfer and carbon fl uxes. Environmental Research, 161(2018), 291–298, DOI: 10.1016/j.envres.2017.11.009.

Chen V.J. and Kuo C.Y. (1986). A study on synthetic sedimentgraphs for ungaged watersheds. Journal of Hydrology, 84(1–2), 35–54.

Choubin B., Darabi H., Rahmati O., Sajedi-Hosseini F. and Kløve B. (2018). River suspended sediment modelling using the CART model: A comparative study of machine learning techniques. Science of the Total Environment, 615, 272–281.

Cimen M. (2008). Estimation of daily suspended sediments using support vector machines. Hydrological Sciences Journal, 53(3), 656–666.

Clark C. o. (1945). Storage and the unit hydrograph. Proceedings of the American Society of Civil Engineer, 69(9), 1333–1360.

Dawson C.W., Abrahart R.J. and See L.M. (2007). HydroTest : A web-based toolbox of evaluation metrics for the standardised assessment of hydrological forecasts. Environmental Modeling & Software, 22(2007), 1034–1052, DOI: 10.1016/j.envsoft.2006.06.008.

De Girolamo A.M., Pappagallo G. and Porto A. Lo. (2015). Temporal variability of suspended sediment transport and rating curves in a Mediterranean river basin: The Celone (SE Italy). Catena, 128, 135–143.

De Paula, D.P., Lima, J.C., Barros, E.L. and Santos, J.D.O. (2021). Coastal erosion and tourism: the case of the distribution of tourist accommodations and their daily rates. Geography, Environment, Sustainability, 14(3), 110-120, DOI: 10.24057/2071-9388-2021-018.

Desmet P.J.J. and Govers G. (1996). A GIS procedure for automatically calculating the USLE LS factor on topographically complex landscape units. Journal of Soil and Water Conservation, 51(5), 427–433.

Du J., Xie H., Hu Y., Xu Y. and Xu C.-Y. (2009). Development and testing of a new storm runoff routing approach based on time variant spatially distributed travel time method. Journal of Hydrology, 369(1–2), 44–54.

Durigon V.L., Carvalho D.F., Antunes M.A.H., Oliveira P.T.S. and Fernandes M.M. (2014). NDVI time series for monitoring RUSLE cover management factor in a tropical watershed. International Journal of Remote Sensing, 35(2), 441–453.

Engman E.T. (1986). Roughness coefficients for routing surface runoff. Journal of Irrigation and Drainage Engineering, 112(1), 39–53.

Fang H. (2020). Impact of land use changes on catchment soil erosion and sediment yield in the northeastern China: A panel data model application. International Journal of Sediment Research, 35(5), 540–549, DOI: 10.1016/j.ijsrc.2020.03.017.

Foster G.R., McCool D.K., Renard K.G. and Moldenhauer W.C. (1981). Conversion of the universal soil loss equation to SI metric units. Journal of Soil and Water Conservation, 36(6), 355–359.

Golosov V.., Zhang X., Qiang T., Zhou P. and He X. (2014). Quantitative assessment of sediment redistribution in the Sichuan hilly basin and the Central Russian upland during the past 60 years. Geography, Environment, Sustainability, 7(3), 39–64.

Gupta S.K., Tyagi J., Singh P.K., Sharma G. and Jethoo A.S. (2019). Soil Moisture Accounting (SMA)based sediment graph models for small watersheds. Journal of Hydrology, 574, 1129–1151, DOI: 10.1016/j.jhydrol.2019.04.077.

Hadjimitsis D.G., Papadavid G., Agapiou A., Themistocleous K., Hadjimitsis M.G. and Retalis A. (2010). Atmospheric correction for satellite remotely sensed data intended for agricultural applications : impact on vegetation indices. 1984, 89–95.

Hadley R.F., Lal R., Onstand C.A., Walling D.E. and Yair A. (1985). Recent developments in erosion and sediment yield studies. Paris. In: International Hydrological Programme, UNESCO.

Hazbavi, Z., Sadeghi, S.H.R., Gholamalifard, M. and Davoudirad, A.A. (2020). Watershed health assessment using pressure-state- response (PSR) framework. Land Degradation and Development, 31, 3-19.

Her Y. and Heatwole C. (2016). HYSTAR Sediment Model: Distributed Two-Dimensional Simulation of Watershed Erosion and Sediment Transport Using Time-Area Routing. Journal of the American Water Resources Association, 52(2), 376–396, DOI: 10.1111/1752-1688.12396

Khaledi Darvishan A., Sadeghi S.H.R. and Gholami L. (2010). Efficacy of Time-Area Method in simulating temporal variation of sediment yield in Chehelgazi watershed , Iran. Annals of Warsaw University of Life Sciences (Land Reclamation), 42(1), 51–60.

Khorsand M., Khaledi Darvishan A. and Gholamalifard M. (2017). Comparison between estimated annual soil lossusing RUSLE model with data from the erosion pins and plots in Khamsan representative watershed. Iranian Journal of Ecohydrology, 3(4), 669–680, DOI: 10.22059/IJE.2016.60376.

Kothyari U. C., Tiwari A.K. and Singh R. (1997). Estimation of temporal variation of sediment yield from small catchments through the kinematic method. Journal of Hydrology, 203(1–4), 39–57, DOI: 10.1016/S0022-1694(97)00084-X.

Kothyari U.C., Tiwari A.K. and Singh R. (1994). prediction of sediment yield. Journal of Irrigation and Drainage Engineering, 120(6), 1122–1131.

Kothyari U.C., Tiwari A.K. and Singh R. (1996). Temporal Variation of Sediment Yield. Journal of Hydrologic Engineering, 1(October), 169–176.

Kothyari UC C, Jain M.K. and Raju K.G.R. (2002). Estimation of temporal variation of sediment yield using GIS. Hydrological Sciences Journal, 47(5), 693–706.

Lee Y.H. and Singh V.P. (2005). Tank model for sediment yield. Water Resources Management, 19(4), 349–362, DOI: 10.1007/s11269-005-7998-y.

Li Z., Xu X., Xu C., Liu M., Wang K. and Yi R. (2017). Monthly sediment discharge changes and estimates in a typical karst catchment of southwest China. Journal of Hydrology, 555, 95–107, DOI: 10.1016/j.jhydrol.2017.10.013.

Mahoney D.T., Fox J.F. and Al Aamery N. (2018). Watershed erosion modeling using the probability of sediment connectivity in a gently rolling system. Journal of Hydrology, 561(April), 862–883, DOI: 10.1016/j.jhydrol.2018.04.034.

Melesse A.M. and Graham W.D. (2004). Storm runoff prediction based on a spatially distributed travel time method utilizing remote sensing and gis. JAWRA Journal of the American Water Resources Association, 40(4), 863–879.

Messina A.M. and Biggs T.W. (2016). Contributions of human activities to suspended sediment yield during storm events from a small, steep, tropical watershed. Journal of Hydrology, 538, 726–742, DOI: 10.1016/j.jhydrol.2016.03.053.

Mirchooli, F., Sadeghi, S.H.R., Khaledi Darvishan, A. and Strobl, J. (2021). Multi-dimensional assessment of watershed condition using a newly developed barometer of sustainability, Science of The Total Environment, 791, 148389, DOI:10.1016/j.scitotenv.2021.148389.

Moore I.D. and Wilson J.P. (1992). Length-slope factors for the Revised Universal Soil Loss Equation : Simplified method of estimation. Journal of Soil and Water Conservation, 47(5), 423–428.

Moradi Dashtpagerdi M., Sadeghi S.H.R. and Moradi Rekabdarkoolai H. (2019). Changeability of simulated watershed hydrographs from different vector scales and cell sizes. Catena, 182, 104097, DOI: 10.1016/j.catena.2019.104097.

Mostafazadeh R., Sadeghi S.H.R. and Sadoddin A. (2015). Analysis of storm-wise sedimentgraphs and rating loops in Galazchai Watershed, West-Azarbaijan. Journal of Water and Soil Conservation, 21(5), 175–190.

Nearing M.A., Foster G.R., Lane L.J. and Finkner S.C. (1989). A process-based soil erosion model for USDA-Water Erosion Prediction Project technology. Transactions of the ASAE, 32(5), 1587–1593.

Nossent J. and Bauwens W. (2012). Application of a normalized Nash-Sutcliffe efficiency to improve the accuracy of the Sobol' sensitivity analysis of a hydrological model. Geophysical Research Abstract EGU General Assembly Conference Abstracts, 14(2011), 237. https://ui.adsabs.harvard.edu/abs/2012EGUGA..14..237N/abstract

Panagos P., Borrelli P., Meusburger K., Zanden E.H. Van Der, Poesen J. and Alewell C. (2015). ScienceDirect Modelling the effect of support practices (P -factor) on the reduction of soil erosion by water at European scale. Environmental Science and Policy, 51(2015), 23–34, DOI: 10.1016/j.envsci.2015.03.012.

Pandey A., Chowdary V.M. and Mal B.C. (2007). Identification of critical erosion prone areas in the small agricultural watershed using USLE , GIS and remote sensing. Water Resources Management Manage, 21(4), 729–746, DOI: 10.1007/s11269-006-9061-z.

Pelton J., Frazier E. and Pickilingis E. (2014). Calculating slope length factor (LS) in the revised Universal Soil Loss Equation (RUSLE).

Qiao L., Liu S., Xue W., Liu P., Hu R., Sun H. and Zhong Y. (2020). Spatiotemporal variations in suspended sediments over the inner shelf of the East China Sea with the effect of oceanic fronts. Estuarine, Coastal and Shelf Science, 234, 106600, DOI: 10.1016/j.ecss.2020.106600

Quijano L., Beguería S., Gaspar L. and Navas A. (2016). Estimating erosion rates using 137Cs measurements and WATEM/SEDEM in a Mediterranean cultivated field. Catena, 138, 38–51.

Rahaman, A.S. and Solavagounder, A. (2020). Natural and human-induced land degradation and its impact using geospatial approach in the Kallar Watershed of Tamil Nadu, India. Geography, Environment, Sustainability, 13(4), 159-175.

Raisi M.B., Sadeghi S.H.R. and Noor H. (2010). Accuracy of Time- Area Method in Sedimentgraph Development in Kojour Watershed. Rangeland, 4(4), 320–333.

Renard K.G., Foster G.R., Weesies G.A. and Porter J.P. (1991). RUSLE: revised universal soil loss equation. Journal of Soil & Water Conservation, 46(1), 30–33.

Rovira A. and Batalla R.J. (2006). Temporal distribution of suspended sediment transport in a Mediterranean basin: The Lower Tordera (NE SPAIN). Geomorphology, 79(1–2), 58–71, DOI: 10.1016/j.geomorph.2005.09.016.

Ruben L.G.D., Szupiany R.N., Latosinski F.G., López Weibel C., Wood M. and Boldt J. (2020). Acoustic Sediment Estimation Toolbox (ASET): A software package for calibrating and processing TRDI ADCP data to compute suspended-sediment transport in sandy rivers. Computers and Geosciences, 140(2020), 104499, DOI: 10.1016/j.cageo.2020.104499

Rymszewicz A., Bruen M., O'Sullivan J.J., Turner J.N., Lawler D.M., Harrington J.R., Conroy E. and Kelly-Quinn M. (2018). Modelling spatial and temporal variations of annual suspended sediment yields from small agricultural catchments. Science of The Total Environment, 619, 672–684.

Sadeghi S.H.R. and Mizuyama T. (2007). Applicability of Modified Universal Soil Loss Equation for prediction of sediment yield in Khanmirza watershed, Iran, Hydrological Science Journal (IAHS), 52(5),1068-1075.

Sadeghi S.H.R. and Saeidi P. (2010). Reliability of sediment rating curves for a deciduous forest watershed in Iran. Hydrological Sciences Journal, 55(5), 821–831.

Sadeghi S.H.R. and Singh J.k. (2005). Development of a synthetic sediment graph using hydrological data. Journal of Agricultural Science and Technology, 7(2005), 69–77.

Sadeghi S.H.R. and Singh V.P. (2017). Dynamics of suspended sediment concentration, flow discharge and sediment particle size interdependency to identify sediment source. Journal of Hydrology, 554(1–2), 100–110, DOI: 10.1016/j.jhydrol.2017.09.006.

Sadeghi S.H.R. and Tavangar S. (2015). Development of stational models for estimation of rainfall erosivity factor in different timescales. Natural Hazards, 77(1), 429–443, DOI: 10.1007/s11069-015-1608-y.

Sadeghi S.H.R. and Tofighi B. (2003). Application of time-area model in preparing sediment rating curve (Case study: Khanmirza River in Karun watershed). Journal of Caspian Agricultural Sciences and Natural Resources, 1(1), 54–66.

Sadeghi S.H.R. and Zakeri M.A. (2015). Partitioning and analyzing temporal variability of wash and bed material loads in a forest watershed in Iran. Journal of Earth System Science, 124(7), 1503–1515.

Sadeghi S.H.R., Mizuyama T., Miyata S., Gomi T. and Kosugi K. (2008). Development , evaluation and interpretation of sediment rating curves for a Japanese small mountainous reforested watershed. Geoderma, 144(2008), 198–211, DOI: 10.1016/j.geoderma.2007.11.008.

Sadeghi S.H.R., Mizuyama T., Miyata S., Gomi T., Kosugi K., Fukushima T., Mizugaki S. and Onda Y. (2008). Determinant factors of sediment graphs and rating loops in a reforested watershed. Journal of Hydrology, 356(3–4), 271–282, DOI: 10.1016/j.jhydrol.2008.04.005.

Sadeghi S.H.R., Mostafazadeh R. and Sadoddin A. (2015). Changeability of simulated hydrograph from a steep watershed resulted from applying Clark's IUH and different time–area histograms. Environmental Earth Sciences, 74(4), 3629–3643, DOI: 10.1007/s12665-015-4426-3.

Sadeghi S.H.R., Saeidi P., Singh V.P. and Telvari A.R. (2019). How persistent are hysteresis patterns between suspended sediment concentration and discharge at different timescales? Hydrological Sciences Journal, 64(15), 1909–1917, DOI: 10.1080/02626667.2019.1676895.

Sadeghi S.H.R., Zabihi, M., Vafakhah M. and Hazbavi Z. (2017). Spatiotemporal mapping of rainfall erosivity index for different return periods in Iran. Natural Hazards, 87(1), 35-56, DOI: 10.1007/s11069-017-2752-3.

Saeedi P., Sadeghi S.H.R. and Telvari A.R. (2016). Sediment graph simulation using Hydrograph. Watershed Engineering and Management, 8(2), 28–41.

Seeger M., Errea M.P., Beguería S., Arnáez J., Martí C. and García-Ruiz J.M. (2004). Catchment soil moisture and rainfall characteristics as determinant factors for discharge/suspended sediment hysteretic loops in a small headwater catchment in the Spanish pyrenees. Journal of Hydrology, 288(3–4), 299–311, DOI: 10.1016/j.jhydrol.2003.10.012.

Singh P.K., Bhunya P.K., Mishra S.K. and Chaube U.C. (2008). A sediment graph model based on SCS-CN method. Journal of Hydrology, 349(1–2), 244–255, DOI: 10.1016/j.jhydrol.2007.11.004.

Singh P.K., Jain M.K. and Mishra S.K. (2013). Fitting a simplified two-parameter gamma distribution function for synthetic sediment graph derivation from ungauged catchments. Arabian Journal of Geosciences, 6(6), 1835–1841, DOI: 10.1007/s12517-011-0473-6.

Sokolov D.I., Erina, O.N., Tereshina M.A. and Puklakov V.V. (2020). Impact of mozhaysk dam on the moscow river sediment transport. Geography, Environment, Sustainability, 13(4), 24-31, DOI: 10.24057/2071-9388-2019-150.

Srivastava A., Brooks E.S., Dobre M., Elliot W.J., Wu J.Q., Flanagan D.C., Gravelle J.A. and Link T.E. (2020). Modeling forest management effects on water and sediment yield from nested , paired watersheds in the interior Pacific Northwest , USA using WEPP. Science of the Total Environment Journal, 701, 134877, DOI: 10.1016/j.scitotenv.2019.134877

Tyagi J. V., Mishra S.K., Singh R. and Singh V.P. (2008). SCS-CN based time-distributed sediment yield model. Journal of Hydrology, 352(3–4), 388–403, DOI: 10.1016/j.jhydrol.2008.01.025.

Usul N. and Yilmaz M. (2002). ESTIMATION OF INSTANTANEOUS UNIT HYDROGRAPH WITH CLARK ' S TECHNIQUE IN GIS. In Proceedings of 2002 ESRI International User Conference. ESRI on-Line, 1–20.

Van Oost K., Govers G. and Desmet P. (2000). Evaluating the effects of changes in landscape structure on soil erosion by water and tillage. Landscape Ecology, 15(6), 577–589.

Van Rompaey A., Bazzoffi P., Jones R.J.A. and Montanarella L. (2005). Modeling sediment yields in Italian catchments. Geomorphology, 65(1–2), 157–169.

Van Rompaey A.J.J., Verstraeten G., Van Oost K., Govers G. and Poesen J. (2001). MODELLING MEAN ANNUAL SEDIMENT YIELD USING A. Earth Surface Processes and Landforms, 26(11), 1221–1236.

Vercruysse K., Grabowski R.C. and Rickson R.J. (2017). Suspended sediment transport dynamics in rivers: Multi-scale drivers of temporal variation. Earth-Science Reviews, 166, 38–52, DOI: 10.1016/j.earscirev.2016.12.016

Verstraeten G., Oost K. Van, Rompaey A. Van, Poesen J. and Govers G. (2002). Evaluating an integrated approach to catchment management to reduce soil loss and sediment pollution through modelling. Soil Use and Management, 18(4), 386–394, DOI: 10.1079/SUM2002150.

Waiyasusri K. and Wetchayont P. (2020). Assessing long-term deforestation in nam san watershed, loei province, Thailand using a dyna-clue model. Geography, Environment, Sustainability, 13(4), 81-97, DOI: 10.24057/2071-9388-2020-14.

Welle P.I. and Woodward D. (1986). Engineering hydrology—Time of concentration. Hydrology Technical Note, No. N4, June 17.

Wischmeier W.H. and Smith D.D. (1978). Predicting rainfall erosion losses: a guide to conservation planning , Issue 537. Department of Agriculture, Science and Education Administration.

Xie H., Shen Z., Chen L., Qiu J. and Dong J. (2017). Time-varying sensitivity analysis of hydrologic and sediment parameters at multiple timescales: Implications for conservation practices. Science of The Total Environment, 598, 353–364.

Yadav A., Chatterjee S. and Equeenuddin S. (2021). Suspended sediment yield modeling in Mahanadi River , India by multi-objective optimization hybridizing arti fi cial intelligence algorithms. International Journal of Sediment Research, 36(1), 76–91, DOI: 10.1016/j.ijsrc.2020.03.018.

Zevenbergen L.W. and Thorne C.R. (1987). quantitative analysis of land surface topography. Earth Surface Processes and Landforms, 12, 47–56.

Zhan W., Wu J., Wei X., Tang S. and Zhan H. (2019). Spatio-temporal variation of the suspended sediment concentration in the Pearl River Estuary observed by MODIS during 2003–2015. Continental Shelf Research, 172, 22–32, DOI: 10.1016/j.csr.2018.11.007.

Zhang X., Estoque R.C. and Murayama Y. (2017). An urban heat island study in Nanchang City, China based on land surface temperature and social-ecological variables. Sustainable Cities and Society, 32, 557–568, DOI: 10.1016/j.scs.2017.05.005.

Zheng F., Zhang X.J., Wang J. and Flanagan D.C. (2020). Assessing applicability of the WEPP hillslope model to steep landscapes in the northern Loess Plateau of China. Soil & Tillage Research, 197(26), 104492, DOI: 10.1016/j.still.2019.104492.

Zheng M., Qin F., Yang J. and Cai Q. (2013). The spatio-temporal invariability of sediment concentration and the flow-sediment relationship for hilly areas of the Chinese Loess Plateau. Catena, 109(2013), 164–176, DOI: 10.1016/j.catena.2013.03.017.

APPENDICES

Appendix Table 1. Details of each isochrone segment and SDR obtained using the Hadley et al. (1985) method for the Galazchai Watershed, Iran

Method	Isochrone NO.	Time of Concentration (min)	Slope (%)	Area (ha)	SDR
Channel longitudinal profile	1	0.25	28.70	91.43	1.00
	2	0.50	34.53	133.69	1.00
	3	0.75	31.90	207.63	0.92
	4	1.00	28.41	270.42	0.89
	5	1.25	24.38	284.55	0.86
	6	1.50	17.82	582.05	0.73
	7	1.75	18.94	939.81	1.00
	8	2.00	24.92	3266.89	1.00
	9	2.25	30.33	1679.44	1.00
	10	2.50	35.31	2722.59	1.00
Spatially Distributed Travel Time	1	0.25	26.70	51.31	1.00
	2	0.50	30.99	132.76	1.00
	3	0.75	31.80	168.48	1.00
	4	1.00	22.91	391.83	0.72
	5	1.25	29.29	615.17	1.00
	6	1.50	29.69	608.41	1.00
	7	1.75	34.01	815.19	1.00
	8	2.00	33.30	959.27	0.97
	9	2.25	26.50	962.88	0.79
	10	2.50	23.95	941.67	0.90
	11	2.75	20.10	1248.58	0.83
	12	3.00	24.12	1363.56	1.00
	13	3.25	27.90	760.55	1.00
	14	3.50	34.13	609.27	1.00
	15	3.75	34.60	562.55	1.00

Appendix Table 2. Characteristics of the storms and details of each isochrone segment and SDR obtained using the WaTEM/SEDEM method for the Galazchai Watershed, Iran

NO.	Date	Rainfall (mm)	Rainfall Erosivity (MJ mm ha^{-1} h^{-1})	Soil Erosion (t ha^{-1})	SDR (Channel longitudinal profile method)										SDR (Spatially distributed travel time method)														
					1	2	3	4	5	6	7	8	9	10	1	2	3	4	5	6	7	8	9	10	11	12	13	14	15
1	29, Oct, 2011	2.42	0.621	0.021	0.551	0.515	0.562	0.593	0.619	0.723	0.709	0.548	0.510	0.478	0.564	0.561	0.607	0.654	0.540	0.490	0.492	0.510	0.570	0.588	0.641	0.576	0.495	0.485	0.470
2	30, Oct, 2011	13.20	1.160	0.039	0.551	0.515	0.562	0.593	0.619	0.723	0.709	0.548	0.510	0.478	0.564	0.561	0.607	0.654	0.540	0.490	0.492	0.510	0.570	0.588	0.641	0.576	0.495	0.485	0.470
3	04, Nov, 2011	13.60	1.180	0.040	0.551	0.515	0.562	0.593	0.619	0.723	0.709	0.548	0.510	0.478	0.564	0.561	0.607	0.654	0.540	0.490	0.492	0.510	0.570	0.588	0.641	0.576	0.495	0.485	0.470
4	05, Nov, 2011	4.62	0.731	0.025	0.551	0.515	0.562	0.593	0.619	0.723	0.709	0.548	0.510	0.478	0.564	0.561	0.607	0.654	0.540	0.490	0.492	0.510	0.570	0.588	0.641	0.576	0.495	0.485	0.470
5	11, Apr, 2012	14.29	1.215	0.041	0.551	0.515	0.562	0.593	0.619	0.723	0.709	0.548	0.510	0.478	0.564	0.561	0.607	0.654	0.540	0.490	0.492	0.510	0.570	0.588	0.641	0.576	0.495	0.485	0.470
6	03, Nov, 2012	8.25	0.913	0.031	0.551	0.515	0.562	0.593	0.619	0.723	0.709	0.548	0.510	0.478	0.564	0.561	0.607	0.654	0.540	0.490	0.492	0.510	0.570	0.588	0.641	0.576	0.495	0.485	0.470
7	11, Nov, 2012	13.50	1.175	0.040	0.551	0.515	0.562	0.593	0.619	0.723	0.709	0.548	0.510	0.478	0.564	0.561	0.607	0.654	0.540	0.490	0.492	0.510	0.570	0.588	0.641	0.576	0.495	0.485	0.470
8	12, Nov, 2012	8.70	0.935	0.032	0.551	0.515	0.562	0.593	0.619	0.723	0.709	0.548	0.510	0.478	0.564	0.561	0.607	0.654	0.540	0.490	0.492	0.510	0.570	0.588	0.641	0.576	0.495	0.485	0.470
9	13, Nov, 2012	14.70	1.235	0.042	0.551	0.515	0.562	0.593	0.619	0.723	0.709	0.548	0.510	0.478	0.564	0.561	0.607	0.654	0.540	0.490	0.492	0.510	0.570	0.588	0.641	0.576	0.495	0.485	0.470
10	14, Nov, 2012	5.18	0.759	0.026	0.551	0.515	0.562	0.593	0.619	0.723	0.709	0.548	0.510	0.478	0.564	0.561	0.607	0.654	0.540	0.490	0.492	0.510	0.570	0.588	0.641	0.576	0.495	0.485	0.470
11	19, Nov, 2012	10.26	1.013	0.034	0.551	0.515	0.562	0.593	0.619	0.723	0.709	0.548	0.510	0.478	0.564	0.561	0.607	0.654	0.540	0.490	0.492	0.510	0.570	0.588	0.641	0.576	0.495	0.485	0.470
12	20, Nov, 2012	3.41	0.671	0.023	0.551	0.515	0.562	0.593	0.619	0.723	0.709	0.548	0.510	0.478	0.564	0.561	0.607	0.654	0.540	0.490	0.492	0.510	0.570	0.588	0.641	0.576	0.495	0.485	0.470
13	25, Nov, 2012	6.40	0.820	0.028	0.551	0.515	0.562	0.593	0.619	0.723	0.709	0.548	0.510	0.478	0.564	0.561	0.607	0.654	0.540	0.490	0.492	0.510	0.570	0.588	0.641	0.576	0.495	0.485	0.470
14	10, Mar, 2014	5.00	0.75	0.025	0.552	0.528	0.571	0.596	0.625	0.720	0.710	0.553	0.516	0.499	0.560	0.569	0.627	0.655	0.544	0.497	0.510	0.521	0.575	0.587	0.644	0.582	0.508	0.509	0.492
15	17, Mar, 2014	4.50	0.73	0.024	0.552	0.528	0.571	0.596	0.625	0.720	0.710	0.553	0.516	0.499	0.560	0.569	0.627	0.655	0.544	0.497	0.510	0.521	0.575	0.587	0.644	0.582	0.508	0.509	0.492
16	18, Mar, 2014	12.50	1.13	0.037	0.552	0.528	0.571	0.596	0.625	0.720	0.710	0.553	0.516	0.499	0.560	0.569	0.627	0.655	0.544	0.497	0.510	0.521	0.575	0.587	0.644	0.582	0.508	0.509	0.492
17	30, Mar, 2014	7.00	0.85	0.028	0.552	0.528	0.571	0.596	0.625	0.720	0.710	0.553	0.516	0.499	0.560	0.569	0.627	0.655	0.544	0.497	0.510	0.521	0.575	0.587	0.644	0.582	0.508	0.509	0.492
18	13, Apr, 2014	4.00	0.70	0.023	0.552	0.528	0.571	0.596	0.625	0.720	0.710	0.553	0.516	0.499	0.560	0.569	0.627	0.655	0.544	0.497	0.510	0.521	0.575	0.587	0.644	0.582	0.508	0.509	0.492
19	18, Apr, 2014	5.50	0.78	0.026	0.552	0.528	0.571	0.596	0.625	0.720	0.710	0.553	0.516	0.499	0.560	0.569	0.627	0.655	0.544	0.497	0.510	0.521	0.575	0.587	0.644	0.582	0.508	0.509	0.492
20	19, Oct, 2014	5.00	0.75	0.027	0.587	0.552	0.602	0.642	0.686	0.759	0.741	0.568	0.469	0.400	0.608	0.585	0.652	0.719	0.590	0.517	0.514	0.519	0.572	0.568	0.627	0.545	0.418	0.397	0.392
21	20, Oct, 2014	5.50	0.78	0.028	0.587	0.552	0.602	0.642	0.686	0.759	0.741	0.568	0.469	0.400	0.608	0.585	0.652	0.719	0.590	0.517	0.514	0.519	0.572	0.568	0.627	0.545	0.418	0.397	0.392
22	02, Nov, 2014	3.50	0.68	0.024	0.587	0.552	0.602	0.642	0.686	0.759	0.741	0.568	0.469	0.400	0.608	0.585	0.652	0.719	0.590	0.517	0.514	0.519	0.572	0.568	0.627	0.545	0.418	0.397	0.392
23	16, Nov, 2014	4.00	0.70	0.025	0.587	0.552	0.602	0.642	0.686	0.759	0.741	0.568	0.469	0.400	0.608	0.585	0.652	0.719	0.590	0.517	0.514	0.519	0.572	0.568	0.627	0.545	0.418	0.397	0.392
24	22, Nov, 2014	6.30	0.82	0.029	0.587	0.552	0.602	0.642	0.686	0.759	0.741	0.568	0.469	0.400	0.608	0.585	0.652	0.719	0.590	0.517	0.514	0.519	0.572	0.568	0.627	0.545	0.418	0.397	0.392
25	13, Dec, 2014	8.00	0.90	0.032	0.587	0.552	0.602	0.642	0.686	0.759	0.741	0.568	0.469	0.400	0.608	0.585	0.652	0.719	0.590	0.517	0.514	0.519	0.572	0.568	0.627	0.545	0.418	0.397	0.392
26	17, Feb, 2018	4.90	0.75	0.028	0.549	0.531	0.576	0.624	0.668	0.748	0.731	0.541	0.446	0.412	0.572	0.571	0.627	0.677	0.558	0.487	0.490	0.496	0.532	0.541	0.626	0.548	0.436	0.419	0.422
27	22, Feb, 2018	13.00	1.15	0.042	0.549	0.531	0.576	0.624	0.668	0.748	0.731	0.541	0.446	0.412	0.572	0.571	0.627	0.677	0.558	0.487	0.490	0.496	0.532	0.541	0.626	0.548	0.436	0.419	0.422
28	09, Mar, 2018	11.00	0.85	0.031	0.549	0.531	0.576	0.624	0.668	0.748	0.731	0.541	0.446	0.412	0.572	0.571	0.627	0.677	0.558	0.487	0.490	0.496	0.532	0.541	0.626	0.548	0.436	0.419	0.422
29	29, Mar, 2018	7.00	0.96	0.035	0.549	0.531	0.576	0.624	0.668	0.748	0.731	0.541	0.446	0.412	0.572	0.571	0.627	0.677	0.558	0.487	0.490	0.496	0.532	0.541	0.626	0.548	0.436	0.419	0.422
30	11, Apr, 2018	9.20	0.81	0.030	0.549	0.531	0.576	0.624	0.668	0.748	0.731	0.541	0.446	0.412	0.572	0.571	0.627	0.677	0.558	0.487	0.490	0.496	0.532	0.541	0.626	0.548	0.436	0.419	0.422
31	12, Apr, 2018	6.23	0.94	0.035	0.549	0.531	0.576	0.624	0.668	0.748	0.731	0.541	0.446	0.412	0.572	0.571	0.627	0.677	0.558	0.487	0.490	0.496	0.532	0.541	0.626	0.548	0.436	0.419	0.422
32	15, Apr, 2018	8.80	0.80	0.030	0.549	0.531	0.576	0.624	0.668	0.748	0.731	0.541	0.446	0.412	0.572	0.571	0.627	0.677	0.558	0.487	0.490	0.496	0.532	0.541	0.626	0.548	0.436	0.419	0.422
33	27, Apr, 2018	6.00	0.78	0.029	0.549	0.531	0.576	0.624	0.668	0.748	0.731	0.541	0.446	0.412	0.572	0.571	0.627	0.677	0.558	0.487	0.490	0.496	0.532	0.541	0.626	0.548	0.436	0.419	0.422
34	08, May, 2018	5.50	1.05	0.039	0.549	0.531	0.576	0.624	0.668	0.748	0.731	0.541	0.446	0.412	0.572	0.571	0.627	0.677	0.558	0.487	0.490	0.496	0.532	0.541	0.626	0.548	0.436	0.419	0.422
35	26, Oct, 2018	8.00	0.90	0.029	0.570	0.545	0.588	0.620	0.657	0.727	0.724	0.565	0.521	0.504	0.586	0.579	0.641	0.688	0.571	0.510	0.512	0.526	0.583	0.595	0.652	0.591	0.513	0.516	0.507
36	31, Oct, 2018	12.00	1.10	0.036	0.570	0.545	0.588	0.620	0.657	0.727	0.724	0.565	0.521	0.504	0.586	0.579	0.641	0.688	0.571	0.510	0.512	0.526	0.583	0.595	0.652	0.591	0.513	0.516	0.507
37	25, Mar, 2019	5.50	0.78	0.032	0.587	0.542	0.549	0.549	0.564	0.672	0.660	0.451	0.402	0.401	0.591	0.576	0.609	0.589	0.482	0.416	0.418	0.418	0.467	0.492	0.561	0.490	0.402	0.407	0.410
38	31, Mar, 2019	13.00	1.15	0.047	0.587	0.542	0.549	0.549	0.564	0.672	0.660	0.451	0.402	0.401	0.591	0.576	0.609	0.589	0.482	0.416	0.418	0.418	0.467	0.492	0.561	0.490	0.402	0.407	0.410

Appendix Table 3. Comparison between principle components of observed and estimated sediment graphs from the channel longitudinal profile method and Hadley et al. (1985) method for calibration stage for the Galazchai Watershed, Iran

NO.	Date	Time to peak (h)		RE (%)	AE (%)	Peak Value (ton)		RE (%)	AE (%)	Base Time (h)		RE (%)	AE (%)	Total Sediment (ton)		RE (%)	AE (%)
		Obs.	Est.			Obs.	Est.			Obs.	Est.			Obs.	Est.		
1	29, Oct 2011	4.5	2.5	44.44	44.44	6.94	153.54	-2112.4	2112.43	10.5	2.5	76.19	76.19	52.26	59.45	-13.76	13.76
2	30, Oct 2011	7	2.5	64.29	64.29	4.33	5007.4	-115546.1	115546.1	19.0	2.5	86.84	86.84	80.84	1938.8	-2298.4	2298.4
3	04, Nov 2011	9	2.5	72.22	72.22	16.23	1938.8	-11846.1	11846.09	20.0	2.5	87.50	87.50	241.01	1330.9	-452.23	452.23
4	05, Nov 2011	6.5	2.5	61.54	61.54	6.89	589.41	-8454.5	8454.5	13.5	2.5	81.48	81.48	82.73	228.21	-175.85	175.85
5	11, Apr 2012	7	2.5	64.29	64.29	49.26	12481.5	-25238.1	25238.1	14.5	2.5	82.76	82.76	773.08	4832.7	-525.13	525.13
6	03, Nov 2012	2.5	2.5	0.00	0.00	2.42	3912.9	-161588.7	161588.7	12.5	2.5	80.00	80.00	23.77	1515.0	-6273.7	6273.7
7	11, Nov 2012	6.5	2.5	61.54	61.54	112.3	8430.0	-7404.67	7404.67	11.5	2.5	78.26	78.26	1075.97	3264.0	-203.36	203.36
8	12, Nov 2012	4.5	2.5	44.44	44.44	205.7	4636.0	-2153.77	2153.77	14.5	2.5	82.76	82.76	2455.41	1795.0	26.90	26.90
9	13, Nov 2012	6.5	2.5	61.54	61.54	324.4	4650.9	-1333.55	1333.55	22.0	2.5	88.64	88.64	7094.69	1800.8	74.62	74.62
10	14, Nov 2012	5	2.5	50.00	50.00	34.20	1079.7	-3057.17	3057.17	23.5	2.5	89.36	89.36	936.46	418.07	55.36	55.36
11	19, Nov 2012	7	2.5	64.29	64.29	20.37	3105.5	-15145.60	15145.60	16.5	2.5	84.85	84.85	291.52	1202.4	-312.47	312.47
12	20, Nov 2012	4.5	2.5	44.44	44.44	3.59	287.27	-7902.05	7902.05	12.5	2.5	80.00	80.00	48.90	111.23	-127.46	127.46
13	25, Nov 2012	3	2.5	16.67	16.67	6.56	1768.2	-26854.56	26854.56	8.5	2.5	70.59	70.59	59.90	684.64	-1042.9	1042.9
14	10, Mar 2014	7	2.5	64.29	64.29	26.62	353.91	-1229.47	1229.47	7.0	2.5	64.29	64.29	75.72	140.44	-85.47	85.47
15	17, Mar 2014	6	2.5	58.33	58.33	20.92	344.47	-1546.61	1546.61	7.0	2.5	64.29	64.29	93.75	136.69	-45.80	45.80
16	18, Mar 2014	7	2.5	64.29	64.29	23.82	533.22	-2138.54	2138.54	18.0	2.5	86.11	86.11	216.52	211.59	2.28	2.28
17	30, Mar 2014	6	2.5	58.33	58.33	32.52	401.09	-1133.36	1133.36	17.0	2.5	85.29	85.29	239.30	159.16	33.49	33.49
18	13, Apr 2014	6	2.5	58.33	58.33	2.66	330.31	-12317.7	12317.7	9.0	2.5	72.22	72.22	20.82	131.07	-529.55	529.55
19	18, Apr 2014	9	2.5	72.22	72.22	14.04	368.06	-2521.51	2521.5	10.0	2.5	75.00	75.00	75.01	146.05	-94.71	94.71
20	19, Oct 2014	23	2.5	89.13	89.13	3652.5	437.49	88.02	88.02	36.0	2.5	93.06	93.06	10028.3	151.32	98.49	98.49
21	20, Oct 2014	11	2.5	77.27	77.27	3652.5	454.99	87.54	87.54	24.0	2.5	89.58	89.58	8788.75	157.37	98.21	98.21
22	02, Nov 2014	3	2.5	16.67	16.67	28.09	396.66	-1312.10	1312.1	5.0	2.5	50.00	50.00	137.19	79.95	41.72	41.72
23	16, Nov 2014	4	2.5	37.50	37.50	21.79	408.32	-1773.9	1773.9	12.0	2.5	79.17	79.17	82.08	141.23	-72.06	72.06
24	22, Nov 2014	4	2.5	37.50	37.50	23.52	478.32	-1933.67	1933.67	12.0	2.5	79.17	79.17	112.89	165.44	-46.55	46.55
25	13, Dec 2014	10	2.5	75.00	75.00	228.08	524.99	-130.18	130.18	12.0	2.5	79.17	79.17	861.39	181.58	78.92	78.92
Mean		6.78	2.50	54.34	54.34	340.8	2122.9	-16579.95	16594.00	14.7	2.5	79.46	79.46	1357.93	839.33	-471.58	512.38
Standard Deviation		3.92	0.00	20.17	20.17	979.8	2952.9	37257.35	37251.10	6.6	0.00	9.41	9.41	2769.67	1151.1	1283.4	1267.7
Coefficient of Variations (%)		57.85	0.00	37.12	37.12	287.5	139.10	-224.71	224.49	45.1	0.00	11.84	11.84	203.96	137.15	-272.16	247.42

Appendix Table 4. Comparison between principle components of observed and estimated sediment graphs from the spatially distributed travel time method and the Hadley et al. (1985) method for calibration stage for the Galazchai Watershed, Iran

NO.	Date	Time to peak (h)		RE (%)	AE (%)	Peak Value (ton)		RE (%)	AE (%)	Base Time (h)		RE (%)	AE (%)	Total sediment (ton)		RE (%)	AE (%)
		Obs.	Est.			Obs.	Est.			Obs.	Est.			Obs.	Est.		
1	29, Oct 2011	4.5	2	55.6	55.6	6.94	49.02	-606.35	606.35	10.50	3.75	64.29	64.29	52.26	66.47	-27.2	27.2
2	30, Oct 2011	7	2	71.4	71.4	4.33	1598.7	-36821.4	36821.4	19.00	3.75	80.26	80.26	80.84	2167.7	-2581.5	2581.5
3	04, Nov 2011	9	2	77.8	77.8	16.23	1097.4	-6661.71	6661.71	20.00	3.75	81.25	81.25	241.01	1488.0	-517.4	517.4
4	05, Nov 2011	6.5	2	69.2	69.2	6.89	188.18	-2631.13	2631.13	13.50	3.75	72.22	72.22	82.73	255.15	-208.4	208.4
5	11, Apr 2012	7	2	71.4	71.4	49.26	3984.9	-7989.50	7989.50	14.50	3.75	74.14	74.14	773.08	5403.2	-598.9	598.9
6	03, Nov 2012	2.5	2	20.0	20.0	2.42	1249.2	-51521.1	51521.1	12.50	3.75	70.00	70.00	23.77	1693.9	-7026.1	7026.1
7	11, Nov 2012	6.5	2	69.2	69.2	112.3	2691.4	-2295.96	2295.96	11.50	3.75	67.39	67.39	1075.97	3606.0	-235.1	235.1
8	12, Nov 2012	4.5	2	55.6	55.6	205.7	1480.1	-619.54	619.54	14.50	3.75	74.14	74.14	2455.41	2006.9	18.3	18.3
9	13, Nov 2012	6.5	2	69.2	69.2	324.4	1484.8	-357.68	357.68	22.00	3.75	82.95	82.95	7094.69	2013.4	71.6	71.6
10	14, Nov 2012	5	2	60.0	60.0	34.20	344.72	-907.97	907.97	23.50	3.75	84.04	84.04	936.46	467.42	50.1	50.1
11	19, Nov 2012	7	2	71.4	71.4	20.37	991.48	-4767.34	4767.34	16.50	3.75	77.27	77.27	291.52	1344.4	-361.2	361.2
12	20, Nov 2012	4.5	2	55.6	55.6	3.59	91.72	-2454.75	2454.75	12.50	3.75	70.00	70.00	48.90	124.36	-154.3	154.3
13	25, Nov 2012	3	2	33.3	33.3	6.56	564.53	-8505.57	8505.57	8.50	3.75	55.88	55.88	59.90	765.46	-1177.9	1177.9
14	10, Mar 2014	7	2	71.4	71.4	26.62	115.26	-332.98	332.98	7.00	3.75	46.43	46.43	75.72	156.74	-106.9	106.9
15	17, Mar 2014	6	2	66.7	66.7	20.92	112.19	-436.28	436.28	7.00	3.75	46.43	46.43	93.75	152.56	-62.7	62.7
16	18, Mar 2014	7	2	71.4	71.4	23.82	173.66	-629.05	629.05	18.00	3.75	79.17	79.17	216.52	236.15	-9.1	9.1
17	30, Mar 2014	6	2	66.7	66.7	32.52	130.63	-301.69	301.69	17.00	3.75	77.94	77.94	239.30	177.63	25.8	25.8
18	13, Apr 2014	6	2	66.7	66.7	2.66	107.58	-3944.4	3944.4	9.00	3.75	58.33	58.33	20.82	146.29	-602.6	602.6
19	18, Apr 2014	9	2	77.8	77.8	14.04	119.87	-753.77	753.77	10.00	3.75	62.50	62.50	75.01	163.01	-117.3	117.3
20	19, Oct 2014	23	3	86.9	86.9	3652.5	126.25	96.54	96.54	36.00	3.75	89.58	89.58	10028.3	168.96	98.3	98.3
21	20, Oct 2014	11	3	72.7	72.7	3652.5	131.30	96.41	96.41	24.00	3.75	84.38	84.38	8788.75	175.72	98.0	98.0
22	02, Nov 2014	3	3	0.0	0.0	28.09	114.46	-307.48	307.48	5.00	3.75	25.00	25.00	137.19	153.19	-11.7	11.7
23	16, Nov 2014	4	3	25.0	25.0	21.79	117.83	-440.75	440.75	12.00	3.75	68.75	68.75	82.08	157.70	-92.1	92.1
24	22, Nov 2014	4	3	25.0	25.0	23.52	138.03	-486.86	486.86	12.00	3.75	68.75	68.75	112.89	184.73	-63.6	63.6
25	13, Dec 2014	10	3	70.0	70.0	228.1	151.50	33.58	33.58	12.00	3.75	68.75	68.75	861.39	202.76	76.5	76.5
Mean		6.78	2.24	59.2	59.20	340.81	694.19	-5341.87	5359.99	14.72	3.75	69.19	69.19	1357.93	939.12	-540.6	575.71
Standard Deviation		3.92	0.43	21.0	21.04	979.77	947.83	11895.41	11887.2	6.64	0.00	14.12	14.12	2769.67	1281.8	1434.3	1420.6
Coefficient of Variations (%)		57.8	19.1	35.5	35.54	287.48	136.54	-222.68	221.78	45.14	0.00	20.40	20.40	203.96	136.49	-265.3	246.75

Appendix Table 5. Comparison between principle components of observed and estimated sediment graphs from the channel longitudinal profile method and WaTEM/SEDEM method for calibration stage for the Galazchai Watershed, Iran

NO.	Date	Time to peak (h)		RE (%)	AE (%)	Peak Value (ton)		RE (%)	AE (%)	Base Time (h)		RE (%)	AE (%)	Total sediment (ton)		RE (%)	AE (%)
		Obs.	Est.			Obs.	Est.			Obs.	Est.			Obs.	Est.		
1	29, Oct 2011	4.5	2.5	44.44	44.44	6.94	146.91	-2016.8	2016.8	10.5	2.50	76.19	76.19	52.26	6.15	88.23	88.23
2	30, Oct 2011	7	2.5	64.29	64.29	4.33	274.42	-6237.6	6237.6	19.0	2.50	86.84	86.84	80.84	11.5	85.79	85.79
3	04, Nov 2011	9	2.5	72.22	72.22	16.23	279.15	-1619.9	1619.9	20.0	2.50	87.50	87.50	241.01	11.7	95.15	95.15
4	05, Nov 2011	6.5	2.5	61.54	61.54	6.89	172.93	-2409.8	2409.8	13.5	2.50	81.48	81.48	82.73	7.24	91.25	91.25
5	11, Apr 2012	7	2.5	64.29	64.29	49.26	287.43	-483.5	483.5	14.5	2.50	82.76	82.76	773.08	12.0	98.44	98.44
6	03, Nov 2012	2.5	2.5	0.00	0.00	2.42	215.99	-8825.0	8825.0	12.5	2.50	80.00	80.00	23.77	9.04	61.96	61.96
7	11, Nov 2012	6.5	2.5	61.54	61.54	112.33	277.97	-147.45	147.45	11.5	2.50	78.26	78.26	1075.9	11.6	98.92	98.92
8	12, Nov 2012	4.5	2.5	44.44	44.44	205.70	221.19	-7.53	7.53	14.5	2.50	82.76	82.76	2455.4	9.26	99.62	99.62
9	13, Nov 2012	6.5	2.5	61.54	61.54	324.43	292.16	9.95	9.95	22.0	2.50	88.64	88.64	7094.7	12.2	99.83	99.83
10	14, Nov 2012	5	2.5	50.00	50.00	34.20	179.55	-425.01	425.01	23.5	2.50	89.36	89.36	936.46	7.52	99.20	99.20
11	19, Nov 2012	7	2.5	64.29	64.29	20.37	239.64	-1076.4	1076.4	16.5	2.50	84.85	84.85	291.52	10.0	96.56	96.56
12	20, Nov 2012	4.5	2.5	44.44	44.44	3.59	158.74	-4321.6	4321.6	12.5	2.50	80.00	80.00	48.90	6.64	86.41	86.41
13	25, Nov 2012	3	2.5	16.67	16.67	6.56	193.98	-2857.1	2857.1	8.5	2.50	70.59	70.59	59.90	8.12	86.44	86.44
14	10, Mar 2014	7	2.5	64.29	64.29	26.62	176.62	-563.5	563.5	7.0	2.50	64.29	64.29	75.72	7.67	89.87	89.87
15	17, Mar 2014	6	2.5	58.33	58.33	20.92	171.91	-721.8	721.8	7.0	2.50	64.29	64.2	93.75	7.47	92.03	92.03
16	18, Mar 2014	7	2.5	64.29	64.29	23.82	266.11	-1017.2	1017.2	18.0	2.50	86.11	86.11	216.52	11.6	94.66	94.66
17	30, Mar 2014	6	2.5	58.33	58.33	32.52	200.17	-515.53	515.53	17.0	2.50	85.29	85.29	239.30	8.70	96.37	96.37
18	13, Apr 2014	6	2.5	58.33	58.33	2.66	164.85	-6097.3	6097.3	9.0	2.50	72.22	72.22	20.82	7.16	65.60	65.60
19	18, Apr 2014	9	2.5	72.22	72.22	14.04	183.69	-1208.3	1208.3	10.0	2.50	75.00	75.00	75.01	7.98	89.36	89.36
20	19, Oct 2014	23	2.5	89.13	89.13	3652.5	174.98	95.21	95.21	36.0	2.50	93.06	93.06	10028	9.48	99.91	99.91
21	20, Oct 2014	11	2.5	77.27	77.27	3652.5	181.98	95.02	95.02	24.0	2.50	89.58	89.58	8788.7	9.86	99.89	99.89
22	02, Nov 2014	3	2.5	16.67	16.67	28.09	158.65	-464.78	464.78	5.0	2.50	50.00	50.00	137.19	8.59	93.74	93.74
23	16, Nov 2014	4	2.5	37.50	37.50	21.79	163.31	-649.49	649.49	12.0	2.50	79.17	79.17	82.08	8.85	89.22	89.22
24	22, Nov 2014	4	2.5	37.50	37.50	23.52	191.31	-713.39	713.39	12.0	2.50	79.17	79.17	112.9	10.4	90.82	90.82
25	13, Dec 2014	10	2.5	75.00	75.00	228.08	209.97	7.94	7.94	12.0	2.50	79.17	79.17	861.4	11.4	98.68	98.68
Mean		6.78	2.50	54.34	54.34	340.81	207.34	-1686.8	1703.5	14.7	2.50	79.46	79.46	1357.9	9.29	91.52	91.52
Standard Deviation		3.92	0.00	20.17	20.17	979.77	45.63	2267.40	2254.9	6.6	0.00	9.41	9.41	2769.7	1.82	9.42	9.42
Coefficient of Variations (%)		57.8	0.00	37.12	37.12	287.48	22.01	-134.42	132.37	45.1	0.00	11.84	11.84	203.96	19.6	10.29	10.29

Appendix Table 6. Comparison between principle components of observed and estimated sediment graphs from the spatially distributed travel time method and WaTEM/SEDEM method for calibration stage for the Galazchai Watershed, Iran

NO.	Date	Time to peak (h)		RE (%)	AE (%)	Peak Value (ton)		RE (%)	AE (%)	Base Time (h)		RE (%)	AE (%)	Total sediment (ton)		RE (%)	AE (%)
		Obs.	Est.			Obs.	Est.			Obs.	Est.			Obs.	Est.		
1	29, Oct 2011	4.5	2	55.56	55.56	6.94	51.17	-637.37	637.37	10.5	3.75	64.29	64.29	52.26	21.24	59.35	59.35
2	30, Oct 2011	7	2	71.43	71.43	4.33	95.59	-2107.6	2107.6	19.0	3.75	80.26	80.26	80.84	39.68	50.91	50.91
3	04, Nov 2011	9	2	77.78	77.78	16.23	97.24	-499.13	499.13	20.0	3.75	81.25	81.25	241.01	40.35	83.26	83.26
4	05, Nov 2011	6.5	2	69.23	69.23	6.89	60.24	-774.28	774.28	13.5	3.75	72.22	72.22	82.73	25.01	69.77	69.77
5	11, Apr 2012	7	2	71.43	71.43	49.26	100.1	-103.25	103.25	14.5	3.75	74.14	74.14	773.08	41.56	94.62	94.62
6	03, Nov 2012	2.5	2	20.00	20.00	2.42	75.24	-3008.9	3008.9	12.5	3.75	70.00	70.00	23.77	31.23	-31.4	31.4
7	11, Nov 2012	6.5	2	69.23	69.23	112.33	96.83	13.80	13.80	11.5	3.75	67.39	67.39	1075.9	40.53	96.23	96.23
8	12, Nov 2012	4.5	2	55.56	55.56	205.70	77.05	62.54	62.54	14.5	3.75	74.14	74.14	2455.4	31.98	98.70	98.70
9	13, Nov 2012	6.5	2	69.23	69.23	324.43	101.8	68.63	68.63	22.0	3.75	82.95	82.95	7094.7	42.25	99.40	99.40
10	14, Nov 2012	5	2	60.00	60.00	34.20	62.55	-82.88	82.88	23.5	3.75	84.04	84.04	936.46	25.96	97.23	97.23
11	19, Nov 2012	7	2	71.43	71.43	20.37	83.48	-309.80	309.80	16.5	3.75	77.27	77.27	291.52	34.65	88.11	88.11
12	20, Nov 2012	4.5	2	55.56	55.56	3.59	55.29	-1440.2	1440.2	12.5	3.75	70.00	70.00	48.90	22.95	53.06	53.06
13	25, Nov 2012	3	2	33.33	33.33	6.56	67.57	-930.06	930.06	8.5	3.75	55.88	55.88	59.90	28.05	53.17	53.17
14	10, Mar 2014	7	2	71.43	71.43	26.62	61.35	-130.47	130.47	7.0	3.75	46.43	46.43	75.72	25.06	66.91	66.91
15	17, Mar 2014	6	2	66.67	66.67	20.92	59.72	-185.45	185.45	7.0	3.75	46.43	46.43	93.75	24.39	73.99	73.99
16	18, Mar 2014	7	2	71.43	71.43	23.82	37.75	-58.49	58.49	18.0	3.75	79.17	79.17	216.52	37.75	82.56	82.56
17	30, Mar 2014	6	2	66.67	66.67	32.52	28.40	12.68	12.68	17.0	3.75	77.94	77.94	239.30	28.40	88.13	88.13
18	13, Apr 2014	6	2	66.67	66.67	2.66	23.39	-779.17	779.17	9.0	3.75	58.33	58.33	20.82	23.39	-12.3	12.3
19	18, Apr 2014	9	2	77.78	77.78	14.04	26.06	-85.60	85.60	10.0	3.75	62.50	62.50	75.01	26.06	65.26	65.26
20	19, Oct 2014	23	3	86.96	86.96	3652.4	30.84	99.16	99.16	36.0	3.75	89.58	89.58	10028	30.84	99.69	99.69
21	20, Oct 2014	11	3	72.73	72.73	3652.4	32.07	99.12	99.12	24.0	3.75	84.38	84.38	8788.7	32.07	99.64	99.64
22	02, Nov 2014	3	3	0.00	0.00	28.09	27.96	0.45	0.45	5.0	3.75	25.00	25.00	137.19	27.96	79.62	79.62
23	16, Nov 2014	4	3	25.00	25.00	21.79	28.79	-32.10	32.10	12.0	3.75	68.75	68.75	82.08	28.79	64.93	64.93
24	22, Nov 2014	4	3	25.00	25.00	23.52	33.72	-43.37	43.37	12.0	3.75	68.75	68.75	112.89	33.72	70.13	70.13
25	13, Dec 2014	10	3	70.00	70.00	228.08	37.01	83.77	83.77	12.0	3.75	68.75	68.75	861.39	37.01	95.70	95.70
Mean		6.78	2.24	59.20	59.20	340.81	58.05	-430.72	465.93	14.72	3.75	69.19	69.19	1357.9	31.24	71.47	74.96
Standard Deviation		3.92	0.43	21.04	21.04	979.77	26.34	744.93	723.43	6.64	0.00	14.12	14.12	2769.7	6.35	31.85	22.41
Coefficient of Variations (%)		57.85	19.1	35.54	35.54	287.48	45.38	-172.95	155.26	45.14	0.00	20.40	20.40	203.96	20.32	44.56	29.89

Appendix Table 7. Comparison between principle components of observed and estimated sediment graphs from the channel longitudinal profile method and the Hadley et al. (1985) method for validation stage for the Galazchai Watershed, Iran

NO.	Date	Time to peak (h)		RE (%)	AE (%)	Peak Value (ton)		RE (%)	AE (%)	Base Time (h)		RE (%)	AE (%)	Total sediment (ton)		RE (%)	AE (%)
		Obs.	Est.			Obs.	Est.			Obs.	Est.			Obs.	Est.		
1	17, Feb 2018	8	2.5	68.75	68.75	13.2	426.91	-3129.27	3129.27	13	2.5	80.77	80.77	21.96	155.3	-607.4	607.4
2	22, Feb 2018	7	2.5	64.29	64.29	56.7	654.6	-1054.50	1054.50	16	2.5	84.38	84.38	89.62	238.2	-165.8	165.8
3	09, Mar 2018	6	2.5	58.33	58.33	30.2	483.84	-1503.71	1503.71	11	2.5	77.27	77.27	158.1	176.1	-11.3	11.3
4	29, Mar 2018	18	2.5	86.11	86.11	78.5	546.45	-595.85	595.85	37	2.5	93.24	93.24	922.7	198.8	78.4	78.4
5	11, Apr 2018	17	2.5	85.29	85.29	18.2	461.07	-2431.96	2431.96	20	2.5	87.50	87.50	166.9	167.8	-0.5	0.5
6	12, Apr 2018	6	2.5	58.33	58.33	3.5	535.07	-15187.7	15187.7	13	2.5	80.77	80.77	33.66	194.7	-478.4	478.4
7	15, Apr 2018	5	2.5	50.00	50.00	20.9	455.38	-2079.89	2079.89	13	2.5	80.77	80.77	112.9	165.7	-46.8	46.8
8	27, Apr 2018	16	2.5	84.38	84.38	62.7	443.99	-608.34	608.34	18	2.5	86.11	86.11	261.4	161.6	38.2	38.2
9	08, May 2018	4	2.5	37.50	37.50	194.9	597.68	-206.69	206.69	11	2.5	77.27	77.27	772.9	217.5	71.9	71.9
10	26, Oct 2018	3	2.5	16.67	16.67	105.8	420.95	-297.84	297.84	19	2.5	86.84	86.84	679.9	165.3	75.7	75.7
11	31, Oct 2018	21	2.5	88.10	88.10	131.4	514.5	-291.67	291.67	33	2.5	92.42	92.42	966.3	202.0	79.1	79.1
12	25, Mar 2019	6	2.5	58.33	58.33	55.5	453.79	-717.64	717.64	16	2.5	84.38	84.38	373.7	178.6	52.21	52.21
13	31, Mar 2019	8	2.5	68.75	68.75	39.9	669.09	-1575.24	1575.24	17	2.5	85.29	85.29	264.2	263.3	0.35	0.35
Mean		9.62	2.5	63.4	63.4	62.4	512.6	-2283.1	2283.1	18.2	2.5	84.4	84.4	371.1	191.1	-70.35	131.2
Standard Deviation		5.84	0.0	20.03	20.03	52.5	80.5	3825.5	3825.5	7.7	0.0	4.8	4.8	329.0	31.3	213.2	182.1
Coefficient of Variations (%)		60.72	0.0	31.6	31.6	83.9	15.7	-167.6	167.6	42.3	0.0	5.7	5.7	88.7	16.4	-303.0	138.8

Appendix Table 8. Comparison between principle components of observed and estimated sediment graphs from the spatially distributed travel time method and the Hadley et al. (1985) method for validation stage for Galazchai Watershed, Iran

NO.	Date	Time to peak (h)		RE (%)	AE (%)	Peak Value (ton)		RE (%)	AE (%)	Base Time (h)		RE (%)	AE (%)	Total sediment (ton)		RE	AE
		Obs.	Est.			Obs.	Est.			Obs.	Est.			Obs.	Est.	(%)	(%)
1	17, Feb 2018	8	2	75.0	75.0	13.22	127.93	-867.70	867.70	13	3.75	71.15	71.15	21.96	173.604	-690.5	690.5
2	22, Feb 2018	7	2	71.4	71.4	56.7	196.16	-245.96	245.96	16	3.75	76.56	76.56	89.62	266.193	-197.0	197.0
3	09, Mar 2018	6	2	66.7	66.7	30.17	144.99	-380.58	380.58	11	3.75	65.91	65.91	158.13	196.752	-24.42	24.42
4	29, Mar 2018	18	2	88.9	88.9	78.53	163.75	-108.52	108.52	37	3.75	89.86	89.86	922.73	222.214	75.92	75.92
5	11, Apr 2018	17	2	88.2	88.2	18.21	138.16	-658.70	658.70	20	3.75	81.25	81.25	166.89	187.493	-12.35	12.35
6	12, Apr 2018	6	2	66.7	66.7	3.5	160.34	-4481.1	4481.1	13	3.75	71.15	71.15	33.66	217.584	-546.4	546.4
7	15, Apr 2018	5	2	60.0	60.0	20.89	136.46	-553.22	553.22	13	3.75	71.15	71.15	112.89	185.178	-64.03	64.03
8	27, Apr 2018	16	2	87.5	87.5	62.68	133.05	-112.26	112.26	18	3.75	79.17	79.17	261.37	180.549	30.92	30.92
9	08, May 2018	4	2	50.0	50.0	194.88	179.10	8.10	8.10	11	3.75	65.91	65.91	772.9	243.046	68.55	68.55
10	26, Oct 2018	3	2	33.3	33.3	105.81	138.09	-30.51	30.51	19	3.75	80.26	80.26	679.89	184.531	72.86	72.86
11	31, Oct 2018	21	2	90.5	90.5	131.36	168.79	-28.49	28.49	33	3.75	88.64	88.64	966.26	219.883	77.24	77.24
12	25, Mar 2019	6	2	66.7	66.7	55.5	152.20	-174.23	174.23	16	3.75	76.56	76.56	373.71	199.478	46.62	46.62
13	31, Mar 2019	8	2	75.0	75.0	39.94	224.40	-461.84	461.84	17	3.75	77.94	77.94	264.23	294.102	-11.31	11.31
Mean		9.6	2.0	70.8	70.8	62.4	158.7	-622.7	623.9	18.2	3.75	76.6	76.6	371.1	213.1	-90.3	147.6
Standard Deviation		5.8	0.0	16.0	16.0	52.4	26.9	1143.8	1143.1	7.7	0.00	7.2	7.2	329.04	34.8	238.3	207.7
Coefficient of Variations (%)		60.7	0.0	22.6	22.6	83.8	16.9	-183.7	183.2	42.3	0.00	9.5	9.5	88.7	16.3	-263.8	140.8

Appendix Table 9. Comparison between principle components of observed and estimated sediment graphs from the channel longitudinal profile method and WaTEM/SEDEM method for validation stage for the Galazchai Watershed, Iran

NO.	Date	Time to peak (h)		RE (%)	AE (%)	Peak Value (ton)		RE (%)	AE (%)	Base Time (h)		RE (%)	AE (%)	Total sediment (ton)		RE (%)	AE (%)
		Obs.	Est.			Obs.	Est.			Obs.	Est.			Obs.	Est.		
1	17, Feb 2018	8	2.5	68.75	68.75	13.22	176.04	-1231.6	1231.6	13	2.50	80.77	80.77	21.96	8.18	62.74	62.74
2	22, Feb 2018	7	2.5	64.29	64.29	56.7	269.93	-376.06	376.06	16	2.50	84.38	84.38	89.62	12.54	86.00	86.00
3	09, Mar 2018	6	2.5	58.33	58.33	30.17	199.51	-561.29	561.29	11	2.50	77.27	77.27	158.13	9.27	94.14	94.14
4	29, Mar 2018	18	2.5	86.11	86.11	78.53	225.33	-186.94	186.94	37	2.50	93.24	93.24	922.73	10.47	98.87	98.87
5	11, Apr 2018	17	2.5	85.29	85.29	18.21	190.12	-944.06	944.06	20	2.50	87.50	87.50	166.89	8.84	94.71	94.71
6	12, Apr 2018	6	2.5	58.33	58.33	3.5	220.64	-6203.9	6203.9	13	2.50	80.77	80.77	33.66	10.25	69.54	69.54
7	15, Apr 2018	5	2.5	50.00	50.00	20.89	187.78	-798.88	798.88	13	2.50	80.77	80.77	112.89	8.73	92.27	92.27
8	27, Apr 2018	16	2.5	84.38	84.38	62.68	183.08	-192.09	192.09	18	2.50	86.11	86.11	261.37	8.51	96.74	96.74
9	08, May 2018	4	2.5	37.50	37.50	194.88	246.46	-26.47	26.47	11	2.50	77.27	77.27	772.9	11.45	98.52	98.52
10	26, Oct 2018	3	2.5	16.67	16.67	105.81	212.22	-100.57	100.57	19	2.50	86.84	86.84	679.89	10.25	98.49	98.49
11	31, Oct 2018	21	2.5	88.10	88.10	131.36	259.38	-97.46	97.46	33	2.50	92.42	92.42	966.26	12.52	98.70	98.70
12	25, Mar 2019	6	2.5	58.33	58.33	55.5	181.80	-227.56	227.56	16	2.50	84.38	84.38	373.71	7.50	97.99	97.99
13	31, Mar 2019	8	2.5	68.75	68.75	39.94	268.04	-571.10	571.10	17	2.50	85.29	85.29	264.23	11.05	95.82	95.82
Mean		9.62	2.50	63.45	63.45	62.41	216.95	-886.00	886.00	18.2	2.50	84.39	84.39	371.10	9.97	91.12	91.12
Standard Deviation		5.84	0.00	20.03	20.03	52.36	32.96	1575.2	1575.2	7.7	0.00	4.83	4.83	329.04	1.56	11.26	11.26
Coefficient of Variations (%)		60.72	0.00	31.57	31.57	83.89	15.19	-177.79	177.79	42.3	0.00	5.72	5.72	88.67	15.67	12.36	12.36

Appendix Table 10. Comparison between principle components of observed and estimated sediment graphs from the spatially distributed travel time method and WaTEM/SEDEM method for validation stage for the Galazchai Watershed, Iran

NO.	Date	Time to peak (h)		RE (%)	AE (%)	Peak Value (ton)		RE (%)	AE (%)	Base Time (h)		RE (%)	AE (%)	Total sediment (ton)		RE (%)	AE (%)
		Obs.	Est.			Obs.	Est.			Obs.	Est.			Obs.	Est.		
1	17, Feb 2018	8	2	75.00	75.00	13.22	64.75	-389.82	389.82	13	3.75	71.15	71.15	21.96	28.37	-29.17	29.17
2	22, Feb 2018	7	2	71.43	71.43	56.7	99.29	-75.12	75.12	16	3.75	76.56	76.56	89.62	43.49	51.47	51.47
3	09, Mar 2018	6	2	66.67	66.67	30.17	73.39	-143.25	143.25	11	3.75	65.91	65.91	158.13	32.15	79.67	79.67
4	29, Mar 2018	18	2	88.89	88.89	78.53	82.89	-5.55	5.55	37	3.75	89.86	89.86	922.73	36.31	96.07	96.07
5	11, Apr 2018	17	2	88.24	88.24	18.21	69.93	-284.05	284.05	20	3.75	81.25	81.25	166.89	30.63	81.64	81.64
6	12, Apr 2018	6	2	66.67	66.67	3.5	81.16	-2218.8	2218.8	13	3.75	71.15	71.15	33.66	35.55	-5.62	5.62
7	15, Apr 2018	5	2	60.00	60.00	20.89	69.07	-230.64	230.64	13	3.75	71.15	71.15	112.89	30.26	73.20	73.20
8	27, Apr 2018	16	2	87.50	87.50	62.68	67.34	-7.44	7.44	18	3.75	79.17	79.17	261.37	29.50	88.71	88.71
9	08, May 2018	4	2	50.00	50.00	194.88	90.66	53.48	53.48	11	3.75	65.91	65.91	772.9	39.71	94.86	94.86
10	26, Oct 2018	3	2	33.33	33.33	105.81	74.19	29.89	29.89	19	3.75	80.26	80.26	679.89	30.22	95.56	95.56
11	31, Oct 2018	21	2	90.48	90.48	131.36	90.67	30.97	30.97	33	3.75	88.64	88.64	966.26	36.93	96.18	96.18
12	25, Mar 2019	6	2	66.67	66.67	55.5	64.95	-17.02	17.02	16	3.75	76.56	76.56	373.71	29.23	92.18	92.18
13	31, Mar 2019	8	2	75.00	75.00	39.94	95.75	-139.75	139.75	17	3.75	77.94	77.94	264.23	43.09	83.69	83.69
Mean		9.62	2.00	70.76	70.76	62.41	78.77	-261.32	278.91	18.23	3.75	76.58	76.58	371.10	34.26	69.11	74.46
Standard Deviation		5.84	0.00	16.02	16.02	52.36	11.62	579.93	571.68	7.71	0.00	7.24	7.24	329.04	5.10	39.02	27.46
Coefficient of Variations (%)		60.72	0.00	22.64	22.64	83.89	14.75	-221.92	204.97	42.28	0.00	9.46	9.46	88.67	14.90	56.46	36.87